NASA Contractor Report 172413

NASA-CR-172413
19840023392

HOOP/COLUMN ANTENNA RF VERIFICATION MODEL

VOLUME II: ANALYSIS AND CORRELATION

W. F. Croswell (Editor), M. D. Vanstrum,
R. J. Schrimpf, R. C. Taylor, and R. L. Moye

HARRIS CORPORATION
Melbourne, Florida

Contract NAS1-15763
August 1984

National Aeronautics and
Space Administration

Langley Research Center
Hampton, Virginia 23665

HOOP/COLUMN ANTENNA
RF VERIFICATION MODEL
ANALYSIS AND CORRELATION

BY

HARRIS Corporation,
Government Electronic Systems Division

Prepared For: Langley Research Center
Under Contract NAS1-15763

EDITOR: W. F. Croswell, Section Head

AUTHORS: M. D. Vanstrum, Senior Engineer

R. J. Schrimpf, Senior Engineer

R. C. Taylor, SAPE

R. L. Moye, Lead Engineer

NOTE

TEST RESULTS FOR HOOP/COLUMN ANTENNA
VERIFICATION MODEL FINAL REPORT COMPRISE
VOLUME I

TABLE OF CONTENTS

VOLUME II

ANALYSIS TECHNIQUES FOR THE QUAD APERTURE REFLECTOR

Introduction

The reflector geometry investigated in the computer analysis portion of this study was the same as that used in the measurement segment, namely, two quadrants of the quad aperture placed side by side. The reflector geometry used in the computer study, and the analysis technique employed, are described below.

Reflector Geometry

Each quadrant of the reflector is fashioned from a paraboloid with a focal point length of 137.7 inches and a radius of 105.32 inches. It should be noted that each quadrant is more than one-quarter of the parent paraboloid. Figures 16 through 18 show the physical dimensions of a single reflector segment. The complete, two-reflector system, is shown in Figure 19, along with the orientation of the global reflector coordinate system to be used in the computer model.

Analytical Method

The technique used to analyze the two quadrant reflector system was the physical optics Surface Current Integration, or SCI method. In this method, the reflector surface is divided into small patches, and the current induced on each patch by the feed is determined. The secondary far-field pattern at each θ, ϕ point desired is the sum of the contribution from each patch. The required inputs to the code implementing this algorithm, are the physical dimensions of the reflector, the location and orientation of the feed, and the co-polarized feed pattern; (in general the entire feed pattern can be included).

The technique used to analyze this problem is similar to the surface current projection scheme described in reference 1. Due to the complex

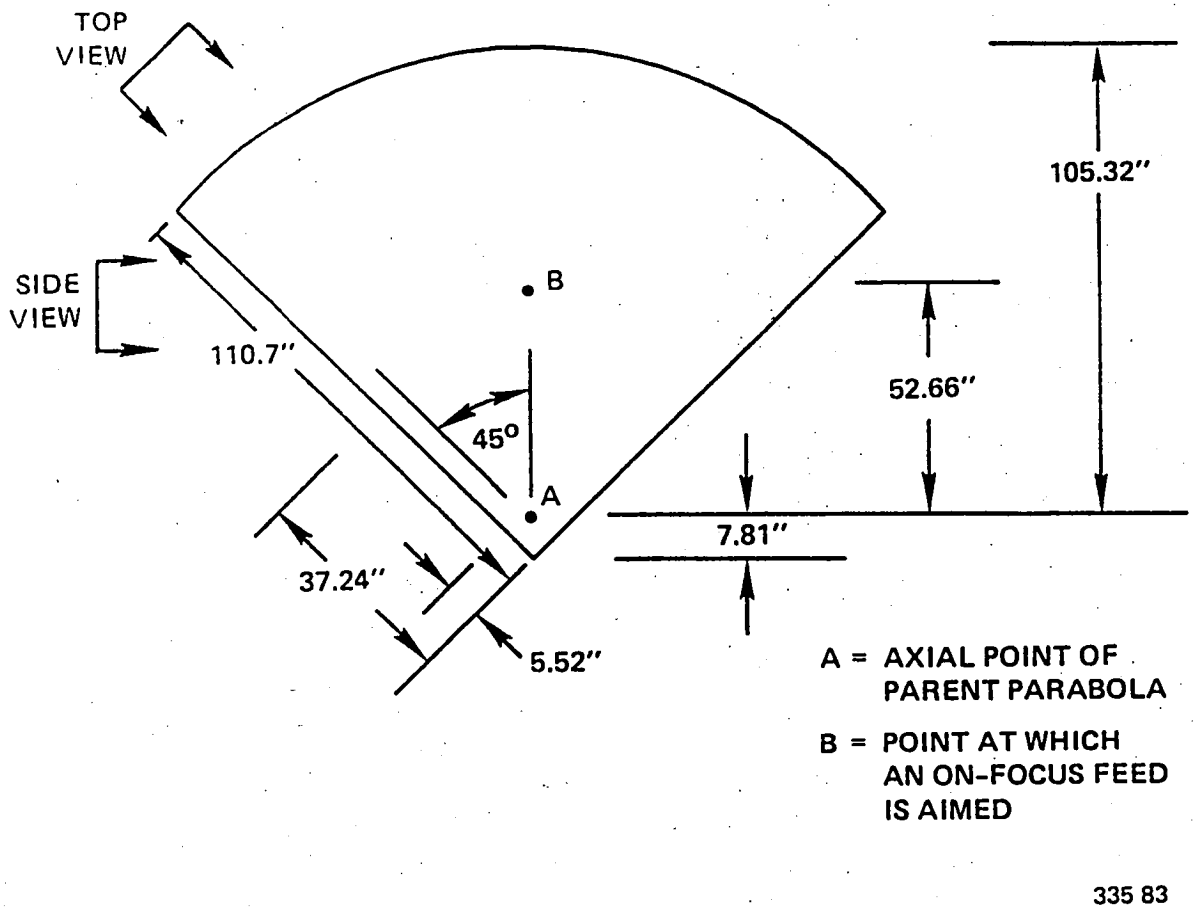

Figure 16. Front View - Quadrant Reflector

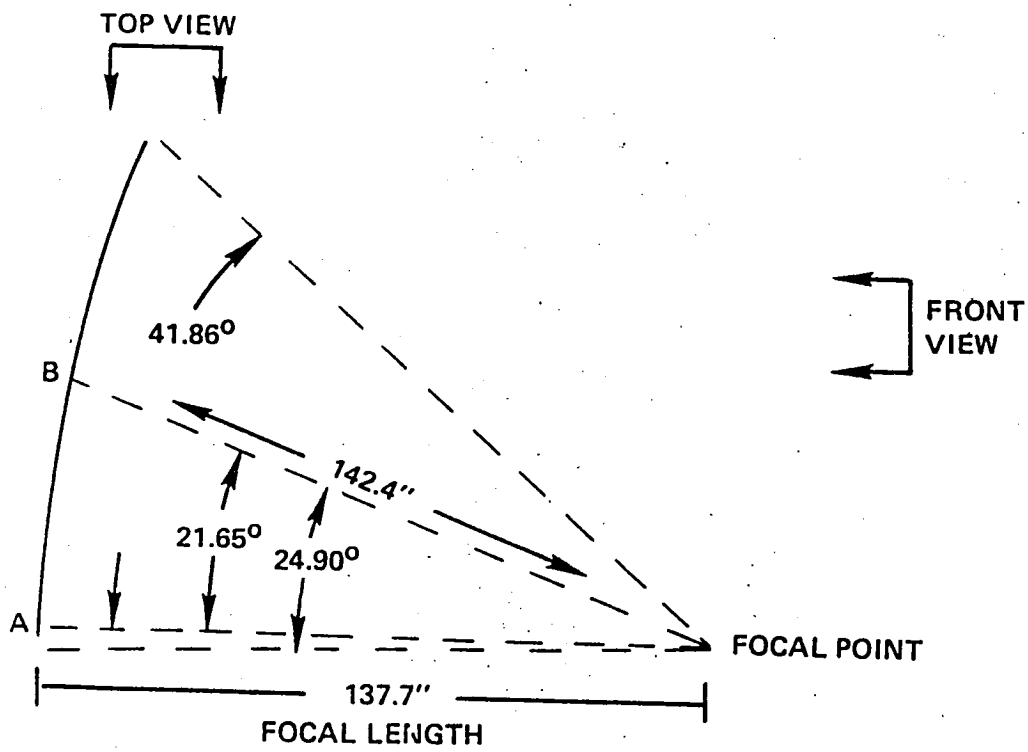

A = AXIAL POINT OF PARENT PARABOLA

B = POINT AT WHICH AN ON-FOCUS FEED IS AIMED

Figure 17. Side View - Quadrant Reflector

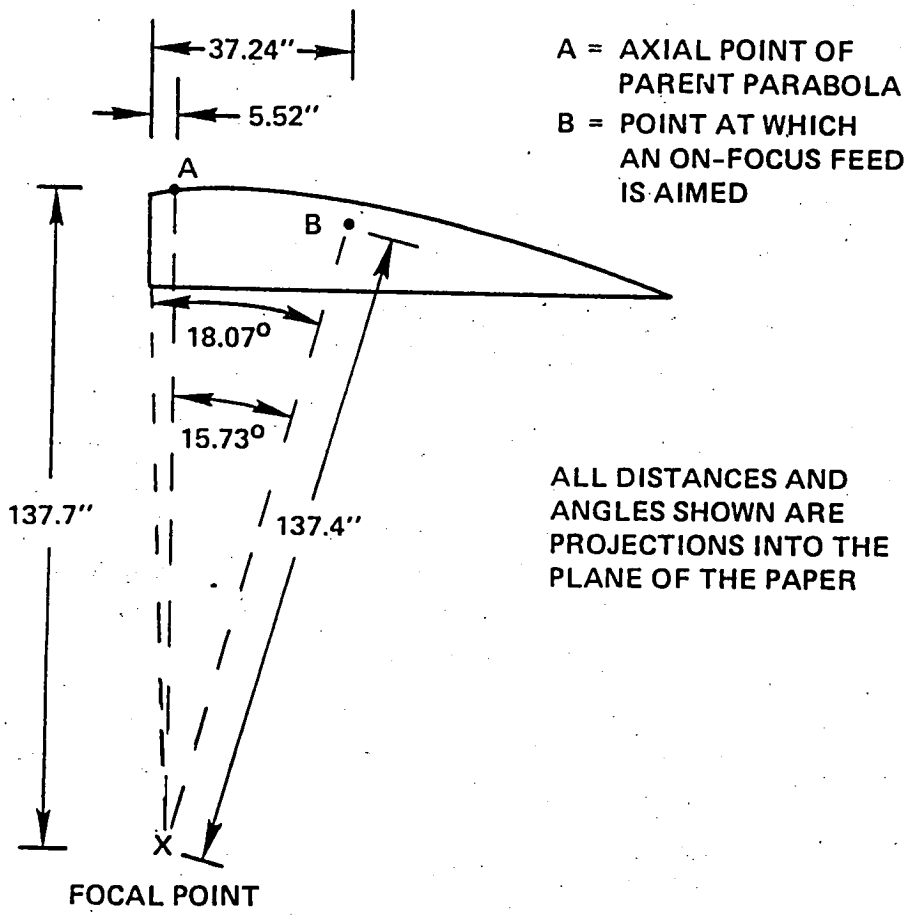

Figure 18. Top View - Quadrant Reflector

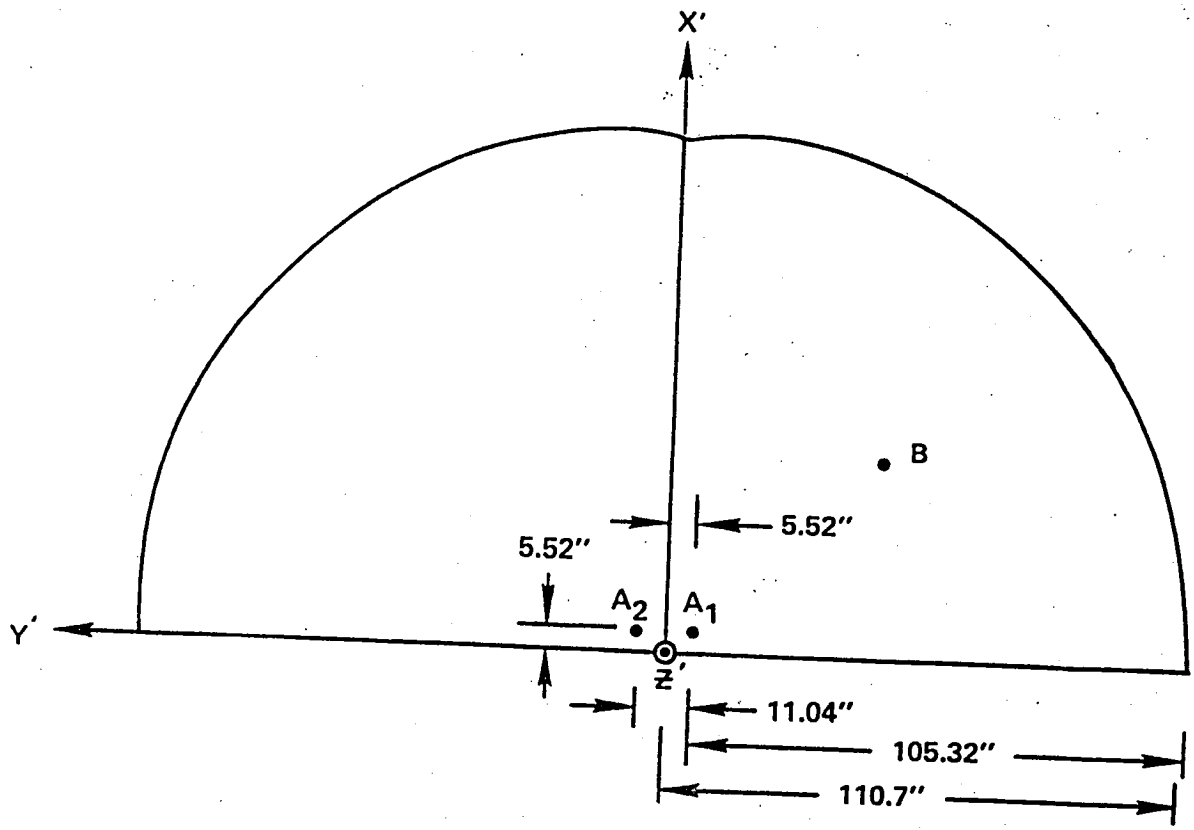

A_1 = AXIAL POINT OF MAIN QUADRANT PARENT PARABOLA

A_2 = AXIAL POINT OF PARASITIC QUADRANT PARENT PARABOLA

B = POINT AT WHICH AN ON-FOCUS FEED IS AIMED

X', Y', Z' = AXES OF REFLECTOR COORDINATE SYSTEM

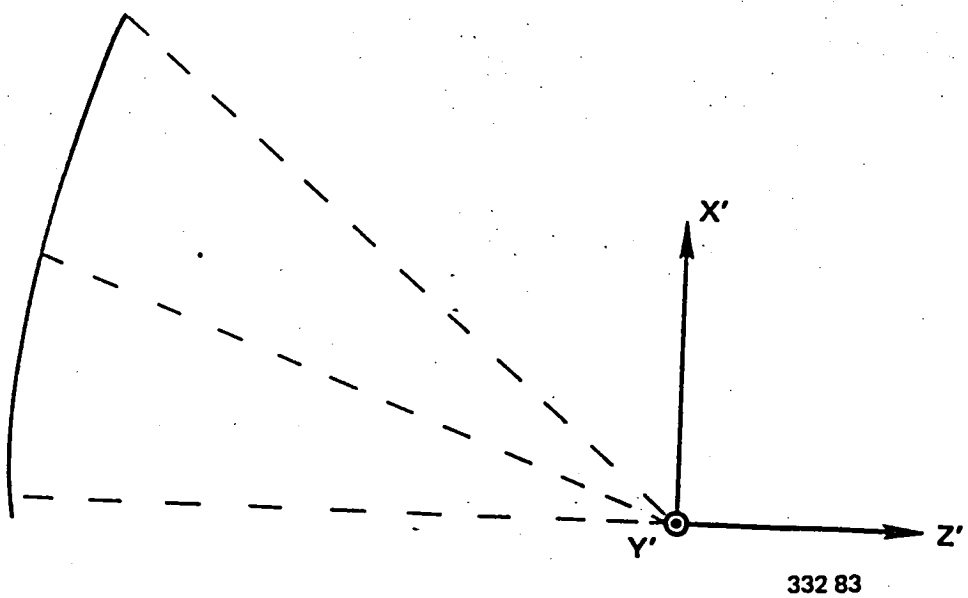

Figure 19. Two Quadrant System

aperture shape, the Jacobi-Bessel expansion, which can improve the running time, was not implemented. The basic geometry of the formulation is shown in Figure 20 where the projection plane chosen is the focal plane of the quad segment. The initial step is to divide the projection of the reflector aperture in the X' - Y' plane into a number of patches. The following operations are then performed for each patch.

1. The center point of each patch on the projected aperture, (ρ', ϕ'), is mapped onto the actual reflector surfaces as point (r', θ', ϕ').
2. A transformation determined by the relative orientation of the feed and reflector coordinate systems is used to transform (r', θ', ϕ') to a point, (r_s, θ_s, ϕ_s), in the feed coordinate system.
3. The magnetic field radiated by the feed at this point is found.
4. The inverse of the transformation in 2) is used to change the magnetic field value to the reflector coordinate system.
5. The surface current density is now found at point (r', θ', ϕ') by

$$\vec{J}(r', \theta', \phi') = 2\hat{n} \times \vec{H}(r', \theta', \phi') \tag{1}$$

Alternately, a projected surface current density can be found at point (ρ', ϕ') by

$$\vec{\tilde{J}}(\rho', \phi') = \vec{2N} \times \vec{H}(r', \theta', \phi') \tag{2}$$

where

$$\hat{n} = \frac{\vec{N}}{|N|} \tag{3}$$

$$\vec{N} = -\frac{\partial N'}{\partial X'}\hat{a}_x - \frac{\partial Z'}{\partial Y'}\hat{a}_y + \hat{a}_z \tag{4}$$

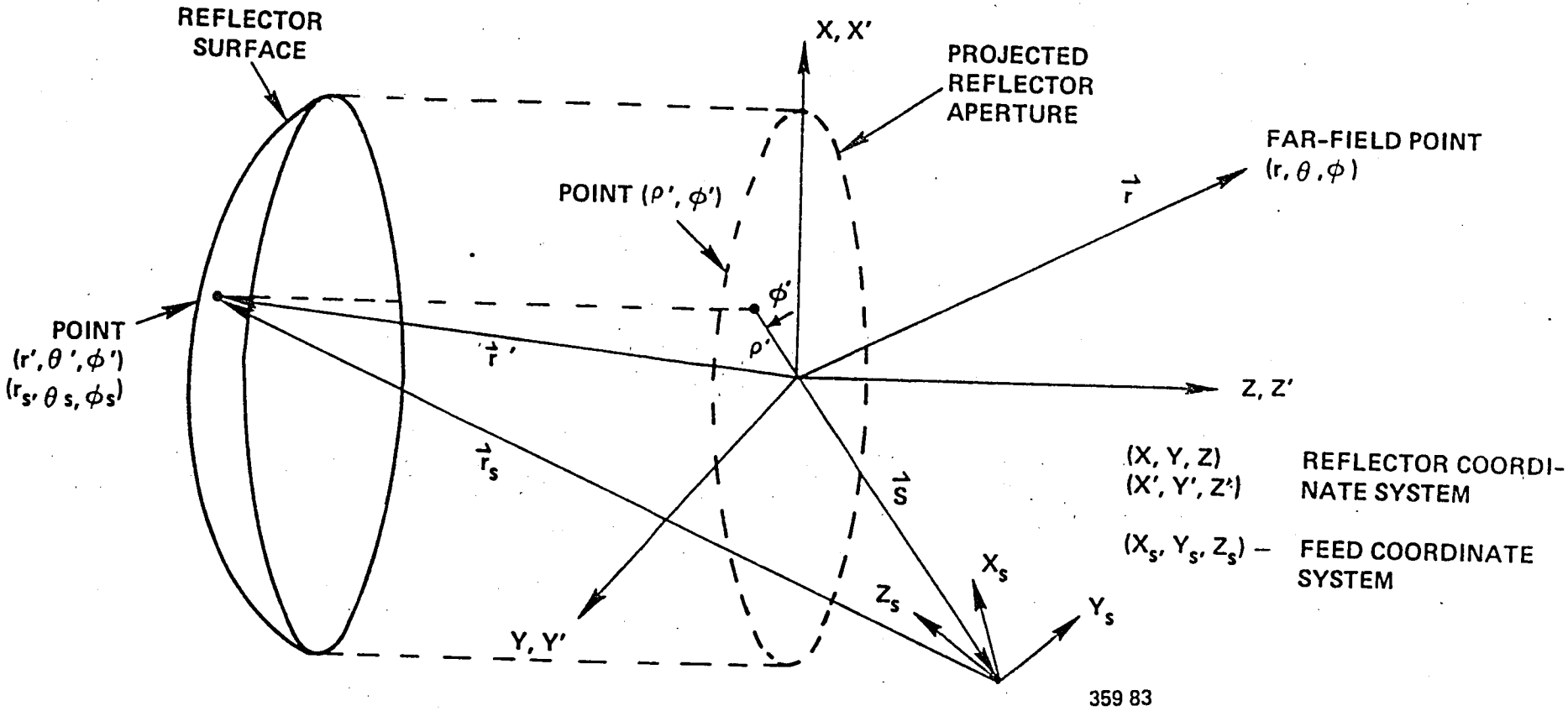

Figure 20. Reflector Antenna Illuminated by an Arbitrarily Located Source

and

$$Z' = \frac{X'^2 + Y'^2}{4f} - f \quad (f = \text{focal distance}) \tag{5}$$

These steps are repeated for each patch on the projected aperture.

Now, the vector potential at the far-field point, $\vec{A}(r, \theta, \phi)$ can be found by

$$\vec{A}(r, \theta, \phi) = \int_{\text{reflector}} \vec{J}(r', \theta', \phi') \frac{e^{-jk|\vec{r} - \vec{r}'|}}{4\pi|r - r'|} ds' \tag{6}$$

This can be approximated in the far field by

$$\vec{T}(\theta, \phi) = \int_{\text{reflector}} \vec{J}(r', \theta', \phi') e^{jk\vec{r} \cdot \hat{a}_{\vec{r}}} ds' \tag{7}$$

or

$$\vec{T}(\theta, \phi) = \int_{\substack{\text{projected} \\ \text{aperture}}} \vec{J}(\rho', \phi') e^{jk\vec{r} \cdot \hat{a}_{\vec{r}}} \rho' \, d\rho' \, d\phi' \tag{8}$$

From this, the far fields can be calculated.

$$\vec{H}(r, \theta, \phi) = \nabla \times \vec{T}(\theta, \phi) \tag{9}$$

$$\vec{E}(r, \theta, \phi) = \frac{1}{j\omega\mu} \nabla \times \vec{H}(r, \theta, \phi) \tag{10}$$

Note that the use of $\vec{J}$ or $\vec{\tilde{J}}$ both result in a surface current integration. A more detailed explanation of this method can be found in [1].

Finally, using the above $\vec{E}$-field, the co-polarized and cross-polarized components of the radiated pattern can be determined. Ludwig's [2] third definition was used in our particular case.

COMPARISON OF MEASURED AND CALCULATED FEED PATTERNS

The feeds used in the RF Verification 5m Model were two pyramidal horns which were designed to have 6 dB and 14 dB edge taper levels on the main quadrant of the dual quad reflector. These two horns are referred to as the 6 dB and 14 dB horns, respectively.

In order to calculate the secondary far-field patterns of the reflector with these horns as feeds, using the physical optics computer program described previously, detailed measured patterns of the horns are required as inputs to the code. The basic horn patterns were measured in the E- and H-planes and the 45 degree plane. In order to conserve computer time, the basic reflector code is written so that it accepts only the principal plane cuts of the feed patterns, with other feed points calculated by a simple interpolation. While this interpolation method is certainly adequate down to the 6 dB or the 14 dB edge field levels, there are questions related to its validity when the E- and H-plane patterns of the feed are asymmetric.

To study this problem, a synthesis of the horn pattern is needed in order to produce the proper raster scan input into the reflector code. The model chosen is the Huygen's source aperture synthesis, where the aperture field is assumed to be the TE_{01} mode expanded from the rectangular waveguide, and weighted with a quadratic phase error related to the horn flare angles.

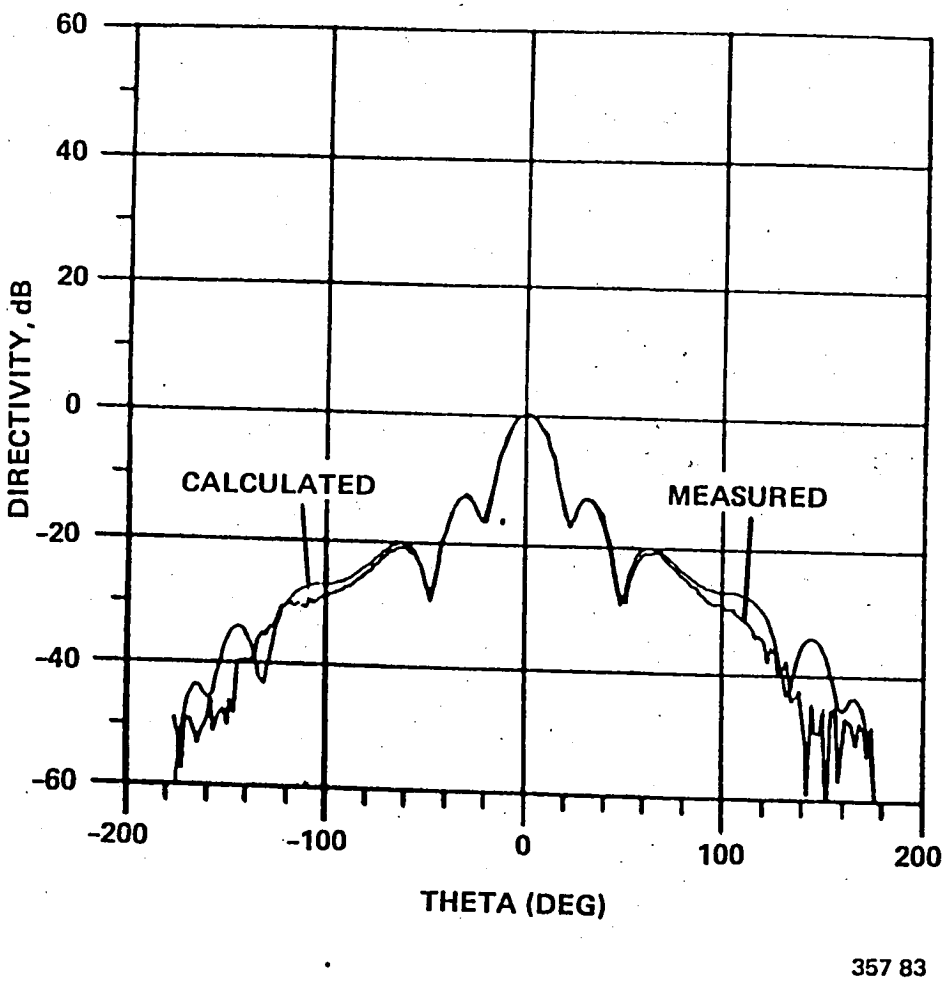

Figure 21. 14 dB Horn E-Plane Measured Versus Calculated Patterns

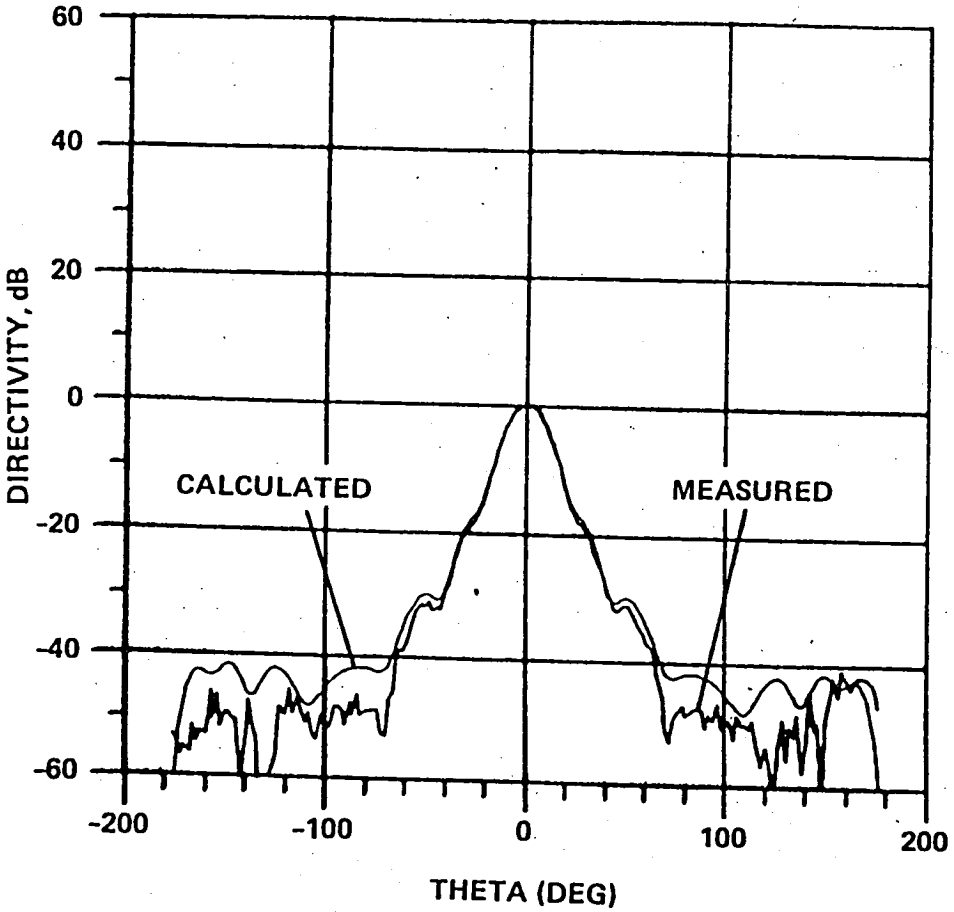

Figure 22. 14 dB Horn H-Plane Measured Versus Calculated Patterns

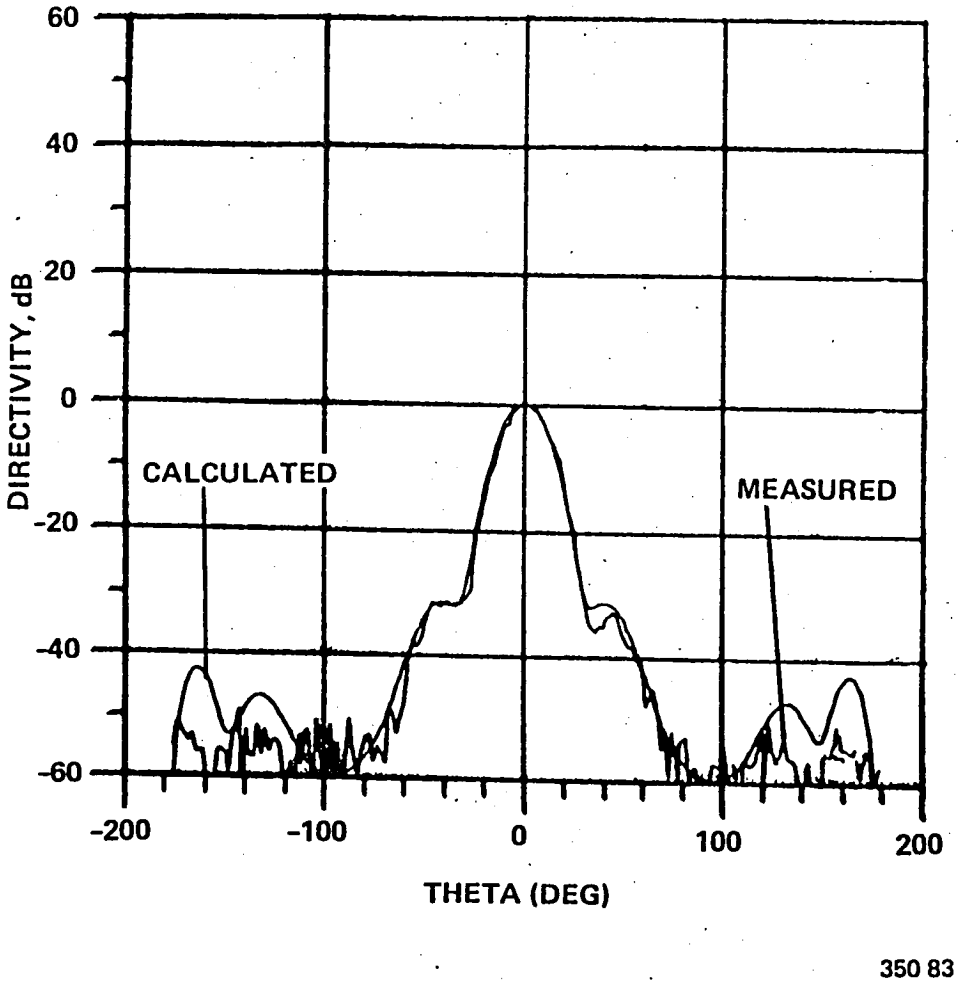

Figure 23. 14 dB Horn 45° Cut Measured Versus Calculated Patterns.

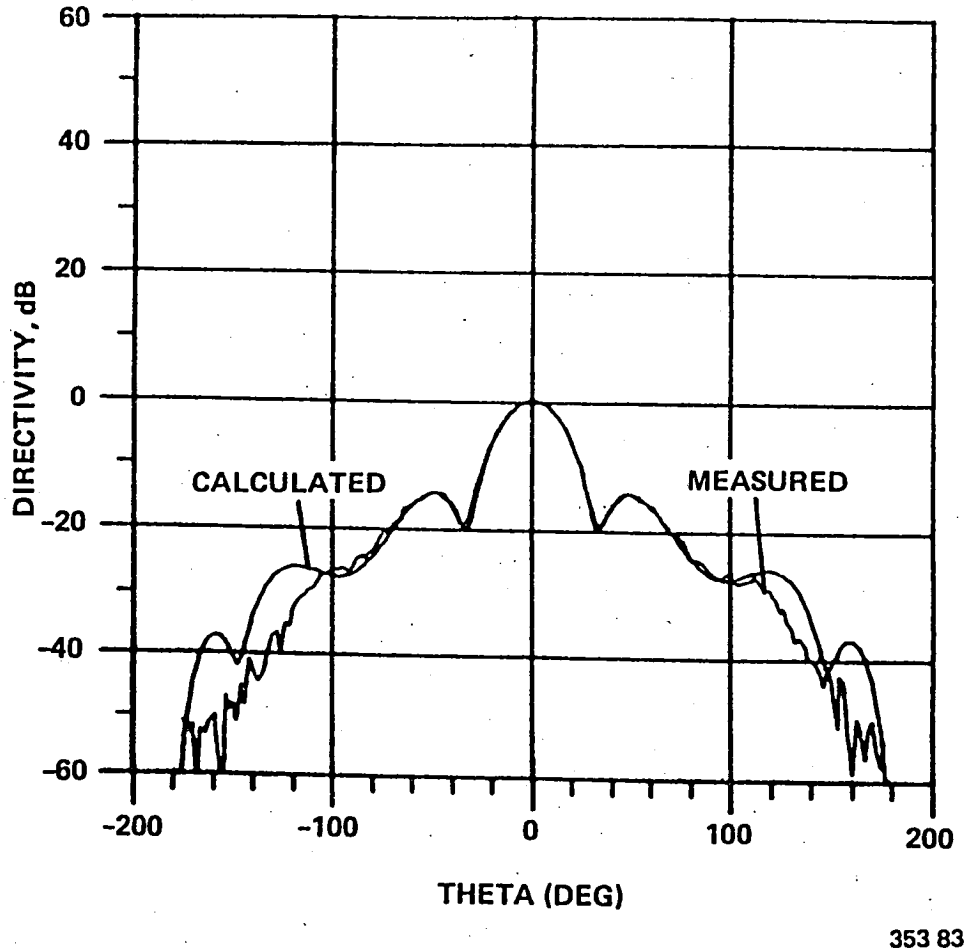

Figure 24. 6 dB Horn E-Plane Measured Versus Calculated Patterns

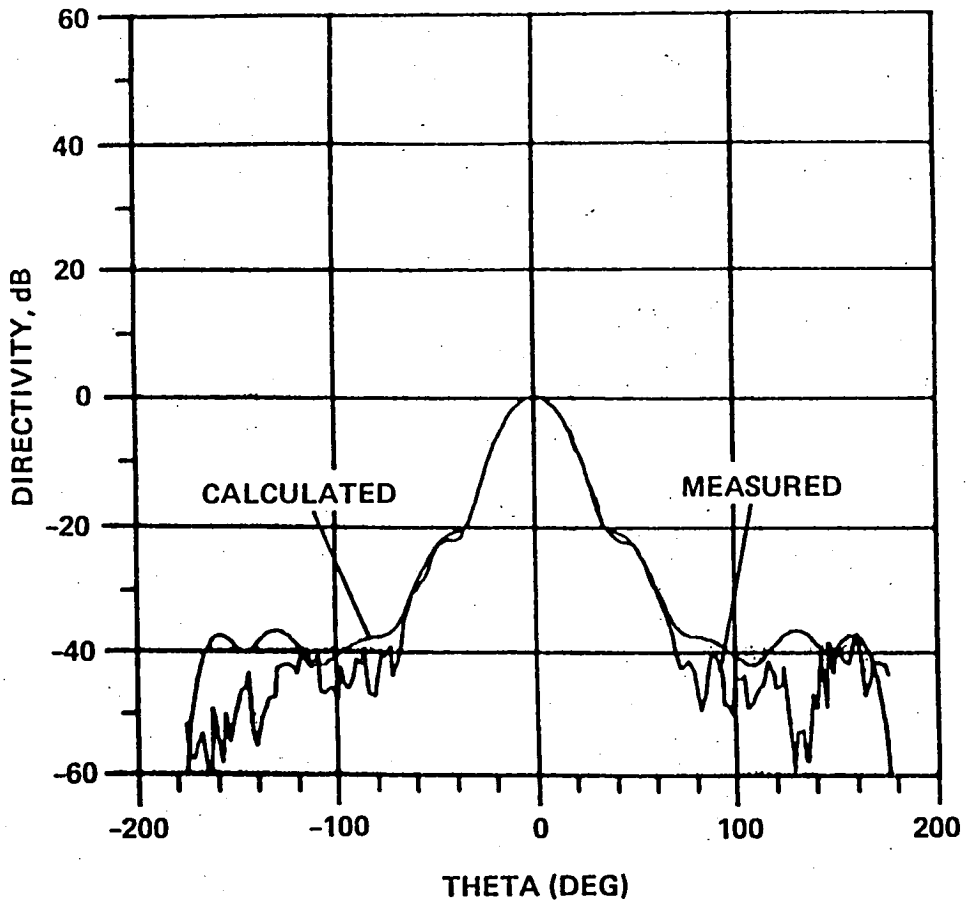

Figure 25. 6 dB Horn H-Plane Measured Versus Calculated Patterns

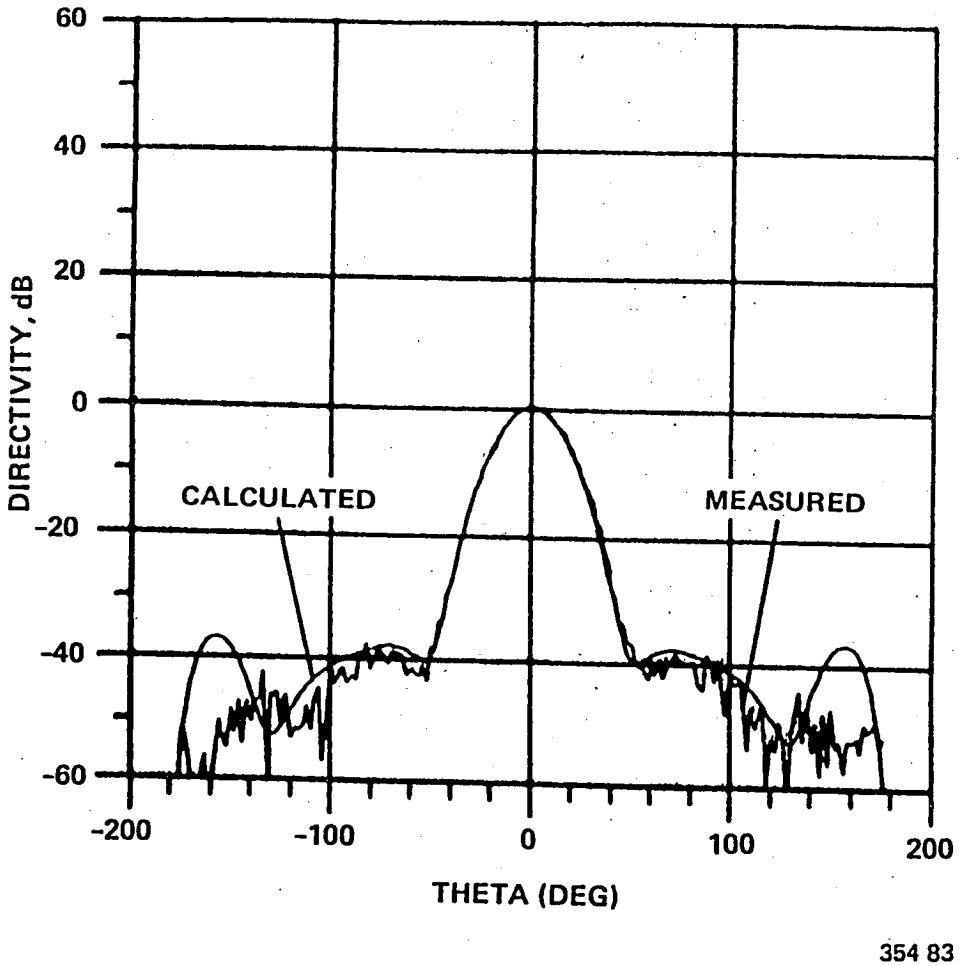

Figure 26. 6 dB 45° Cut Measured Versus Calculated Patterns

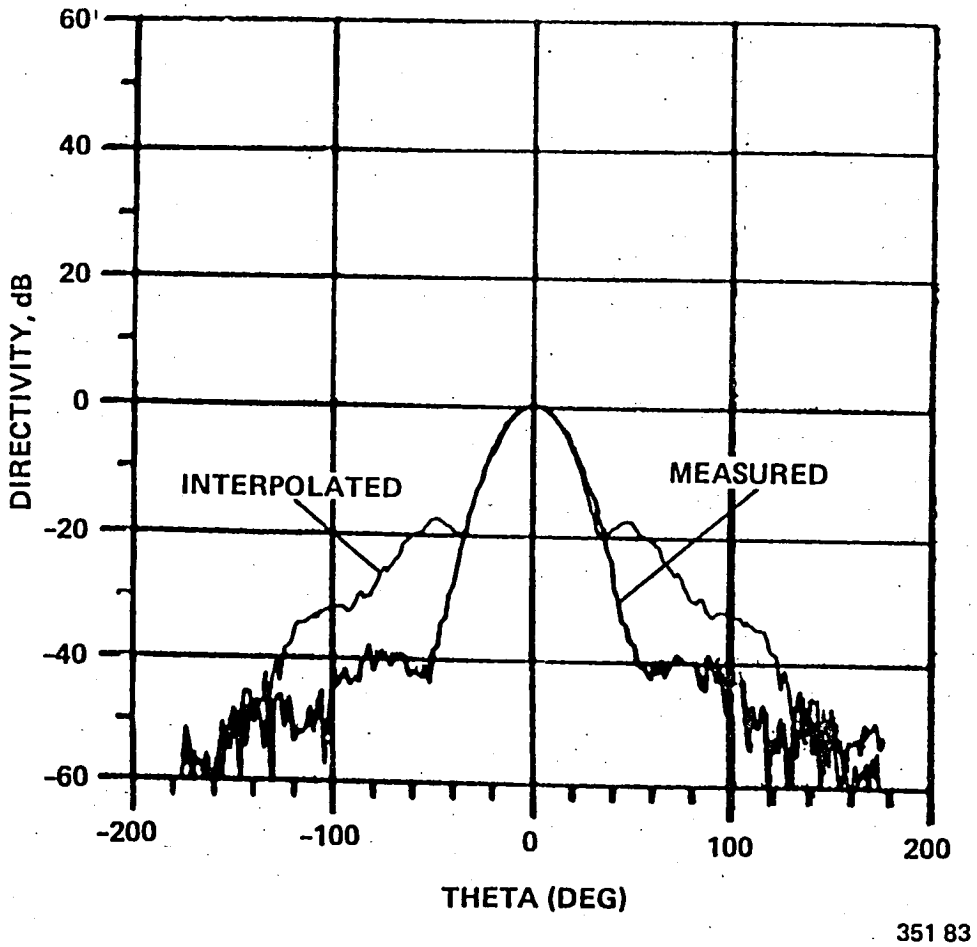

Figure 27. 6 dB 45^{o} Cut Measured Versus Interpolated Patterns

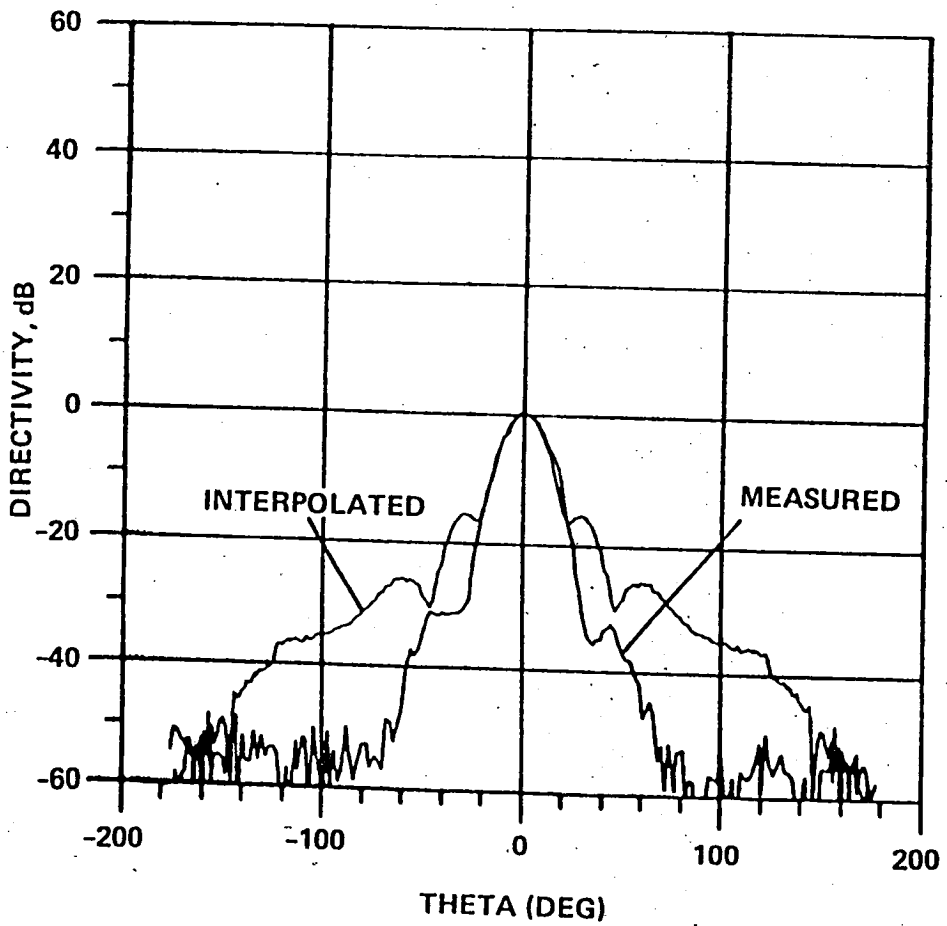

Figure 28. 14 dB Horn 45° Cut Measured Versus Interpolated Patterns

The detailed E-plane, H-plane, and 45° plane patterns calculated using this aperture analysis are given in Figures 21 through 26 and are compared with measured data. The excellent agreement of the analysis with experimental results certainly validates this approximate model for generating detailed feed pattern data. Now let us compare the measured versus interpolated 45° plane data for both the 6 dB and 14 dB horns, given in Figures 27 and 28. Notice that the patterns agree quite well for angles out to 25°. This means that the approximation used in the interpolation is adequate for the primary quad aperture. It is clear that the patterns tend to deviate for angles greater than 25°, particularly for the 14 dB horn case. This error in the input data will produce two effects: (1) the directivity of the feed horn will be inaccurate, where the inaccuracy is estimated to be about 2.5 dB and (2) the scattering patterns of the other quad apertures will be in error. In order to place a bound on this error, several approximations are used in the interpolation of the measured E- and H-plane patterns used in the determination of the far-field secondary patterns which will be presented later.

As a final comment, it is noted that the interpolation error and its significance were not recognized until late in this program when resources were insufficient to both correct the format of the input data, and to generate the lengthy raster scan data for the 6 dB and 14 dB horns.

COMPARISON OF MEASURED AND CALCULATED SECONDARY PATTERNS

To verify the previously measured data, and to validate the Harris reflector code, far-field secondary patterns were calculated using the 6 dB and 14 dB horns as the fed elements. Antenna patterns were computed for each quadrant alone and for the composite reflector. The code corroborates the shape of the main lobe and the presence and location of a large parasitic side lobe due to the off-focus quadrant.

Figures 29, 30, and 31 show wide angle comparisons of the 6 dB horn feed single and double quadrant configurations. A more detailed comparison is shown in Figure 32.

A similar comparison is now presented for the 14 dB horn. Wide angle views are shown in Figures 33, 34, and 35, and a detailed comparison in Figure 36.

One will probably notice some discrepancy in peak gain and parasitic side lobe level. This may be due to several things, including misalignment during measurement and inadequate feed data input to the code (resulting in only approximate intermediate feed points via interpolation).

In order to test this hypothesis, far-field patterns were calculated using an H-plane symmetric (for both the 6 dB and 14 dB horns) feed pattern, as mentioned in an earlier section. The results of this experiment are shown below. Figures 37 and 38 show wide angle and detailed comparisons for the 6 dB feed, dual quadrant case, while the same is shown for the 14 dB feed in Figures 39 and 40. There is some improvement in the agreement between measured and calculated patterns using these feed patterns, especially in the case of the 14 dB horn, which had more asymmetric E- and H-plane patterns to begin with. As suggested earlier, precision agreement may be possible when detailed raster scan measurements are used as input data.

A summary of peak gain and parasitic side lobe level is given in Table I.

In conclusion, it appears that the Harris computer code predicts measured data quite well, especially for those feeds with symmetric E- and H-plane patterns. Since the more elaborate feeds to be investigated later do have symmetric patterns, this analysis should be more than adequate for design purposes.

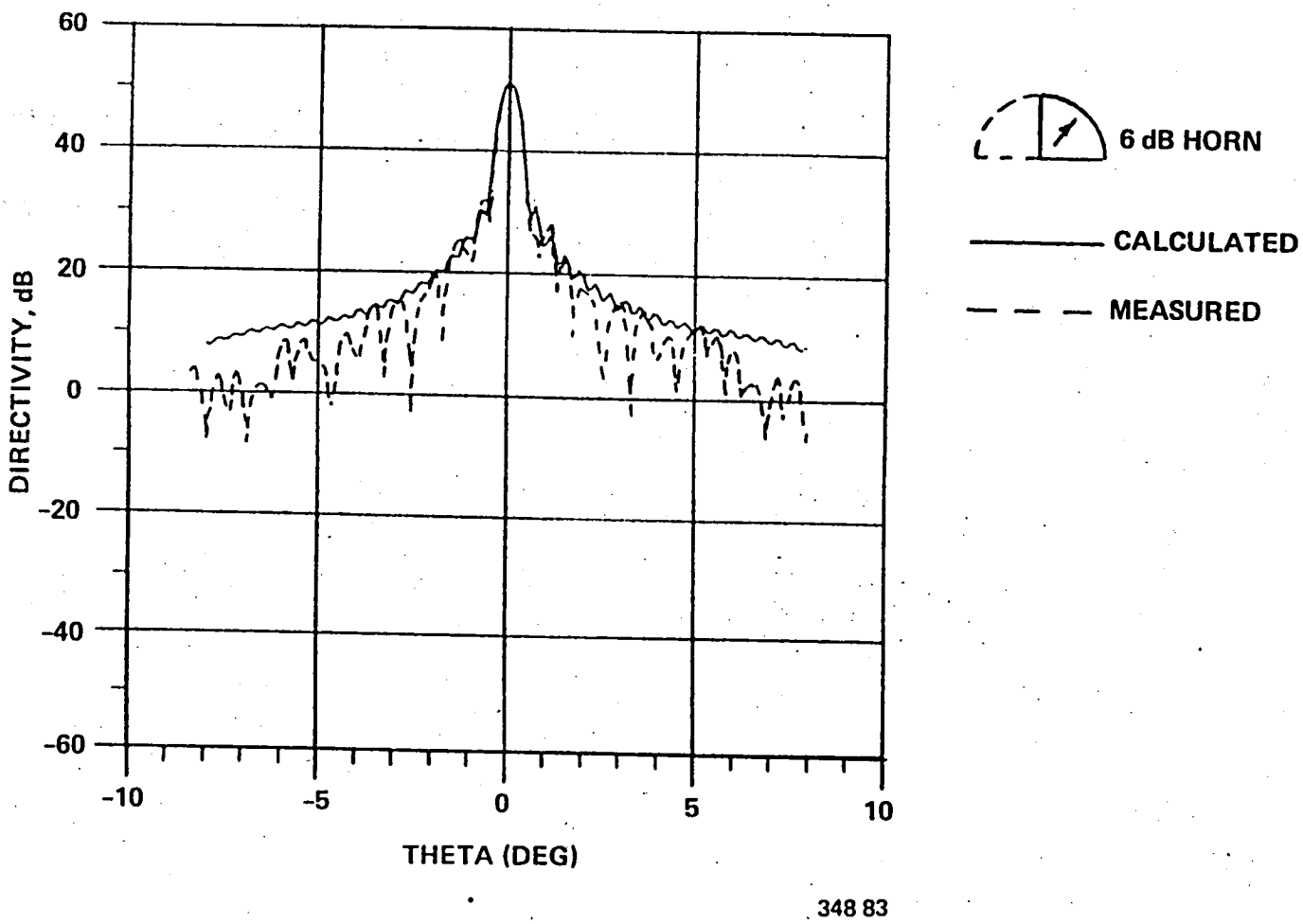

Figure 29. Main Reflector with 6 dB Horn Feed

(E- and H-Planes Asymmetric)

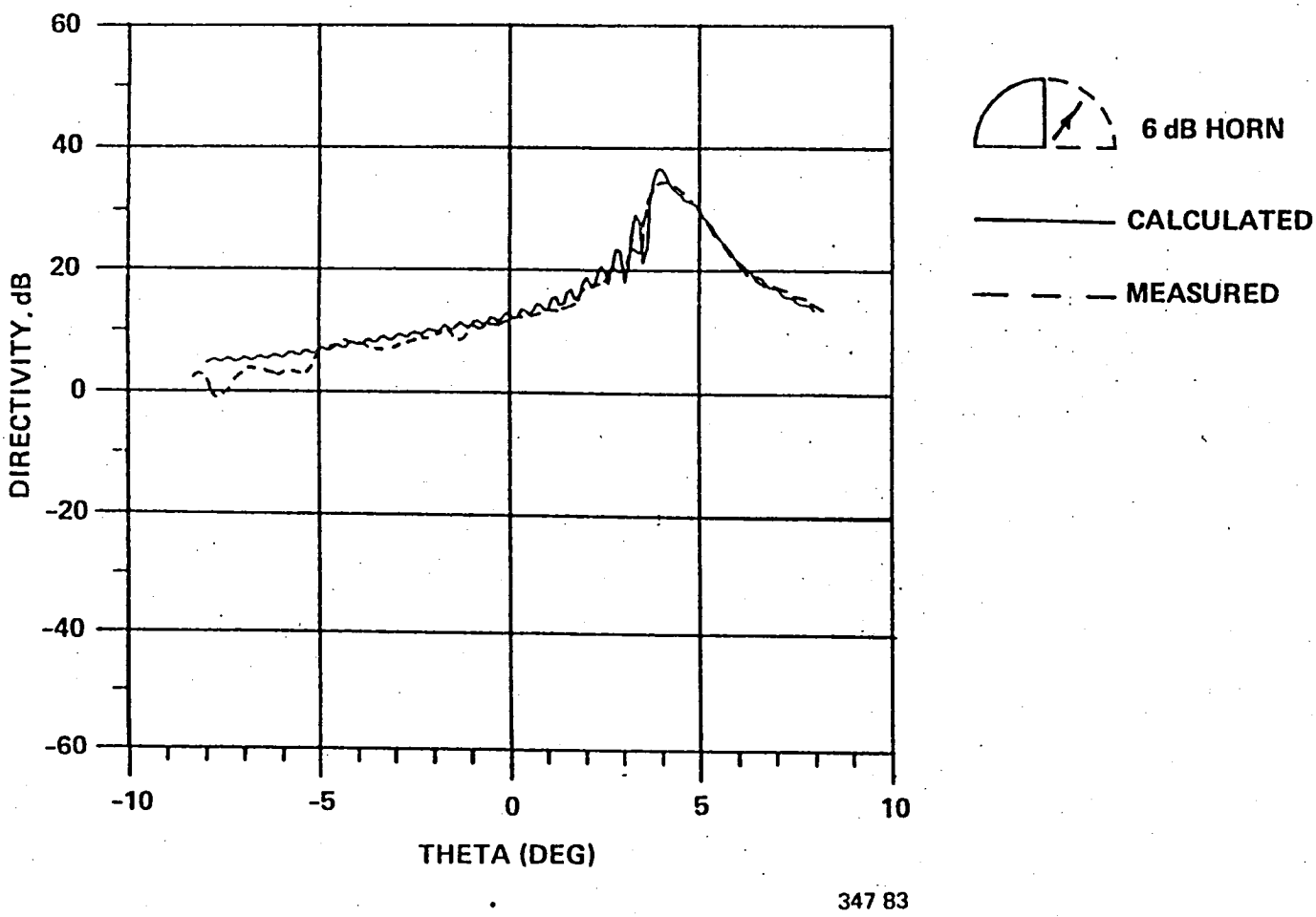

Figure 30. Parasitic Reflector with 6 dB Horn Feed

(E- and H-Planes Asymmetric)

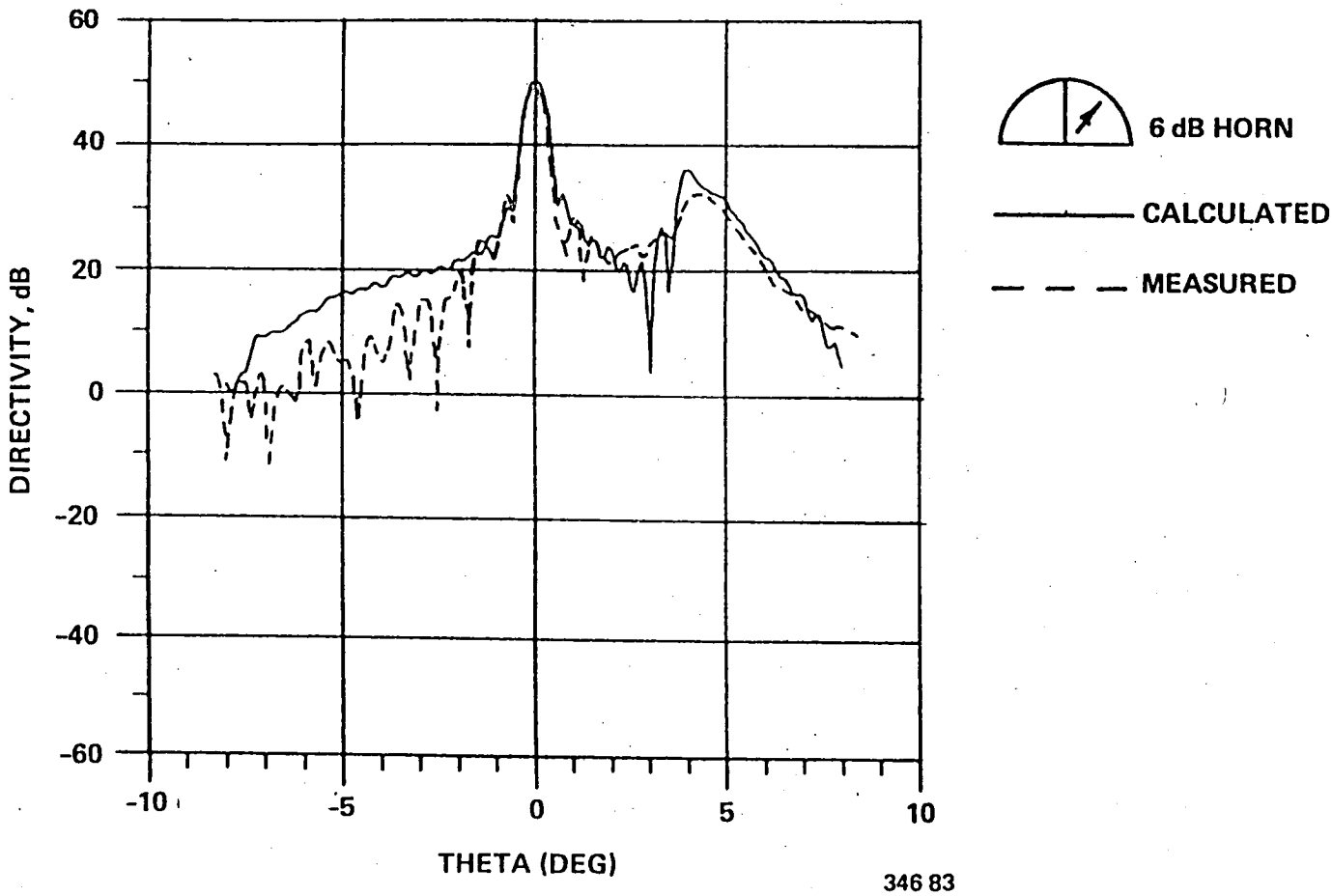

Figure 31. Dual Reflectors with 6 dB Horn Feed

(E- and H-Planes Asymmetric)

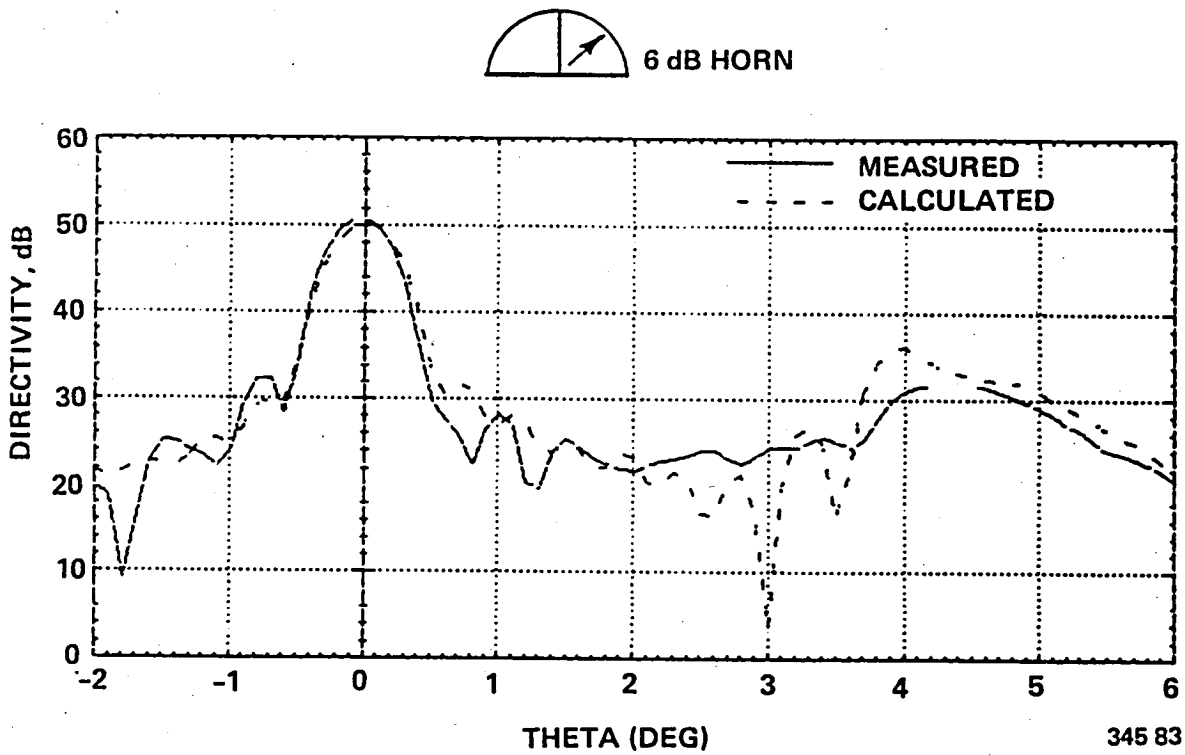

Figure 32. Dual Reflectors with 6 dB Horn Feed

(E- and H-Planes Asymmetric)

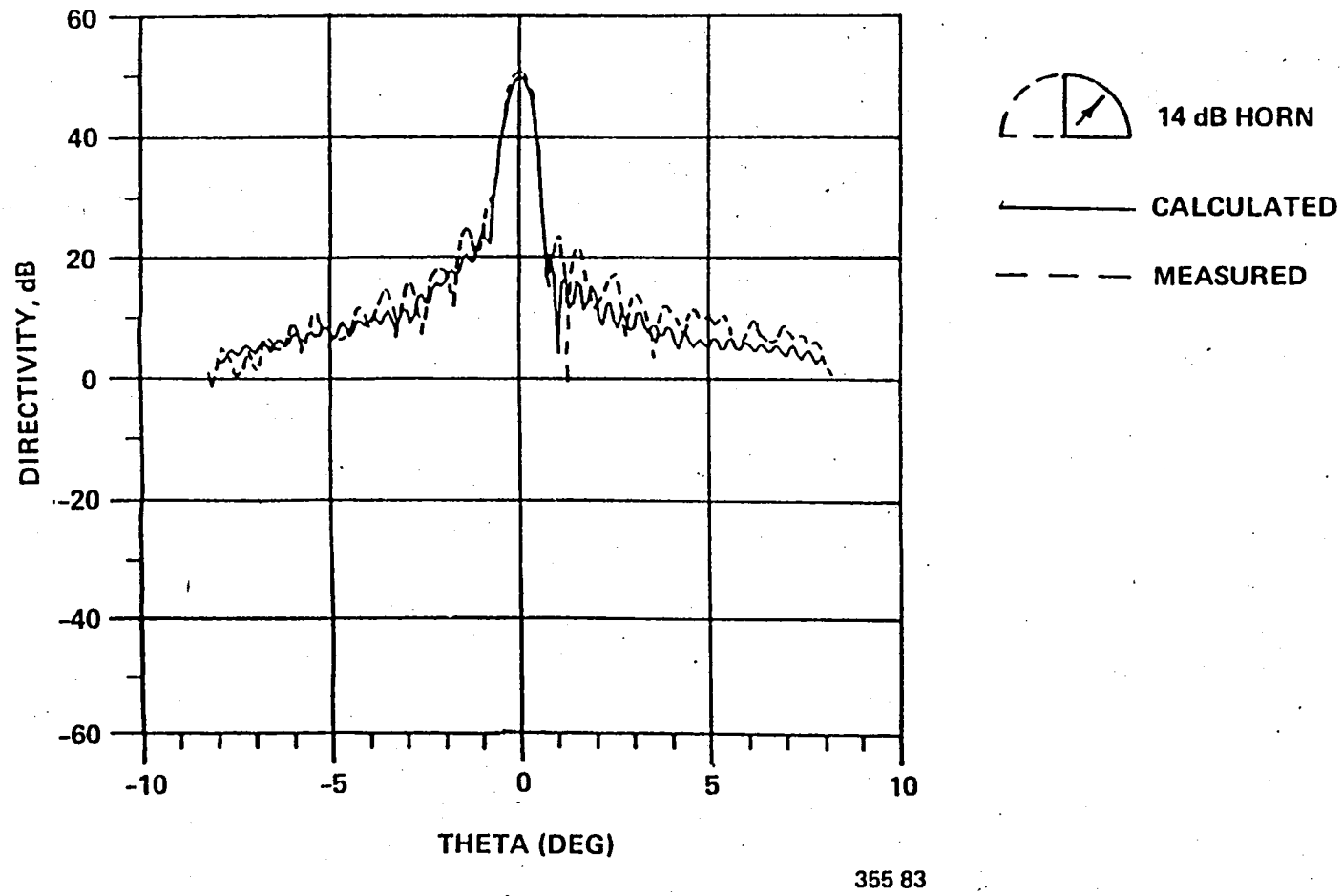

Figure 33. Main Reflector with 14 dB Horn Feed

(E- and H-Planes Asymmetric)

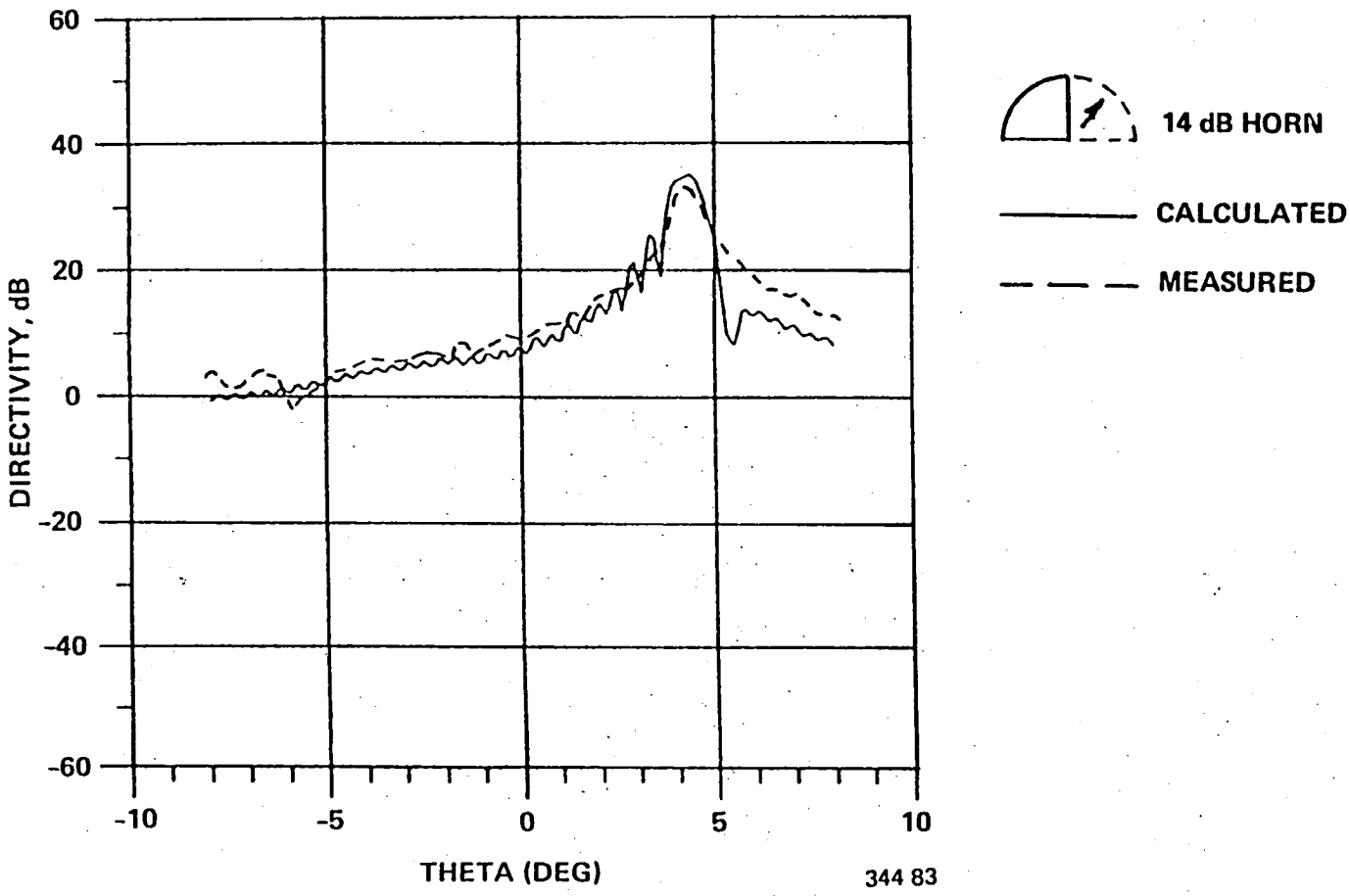

Figure 34. Parasitic Reflector with 14 dB Horn Feed

(E- and H-Planes Asymmetric)

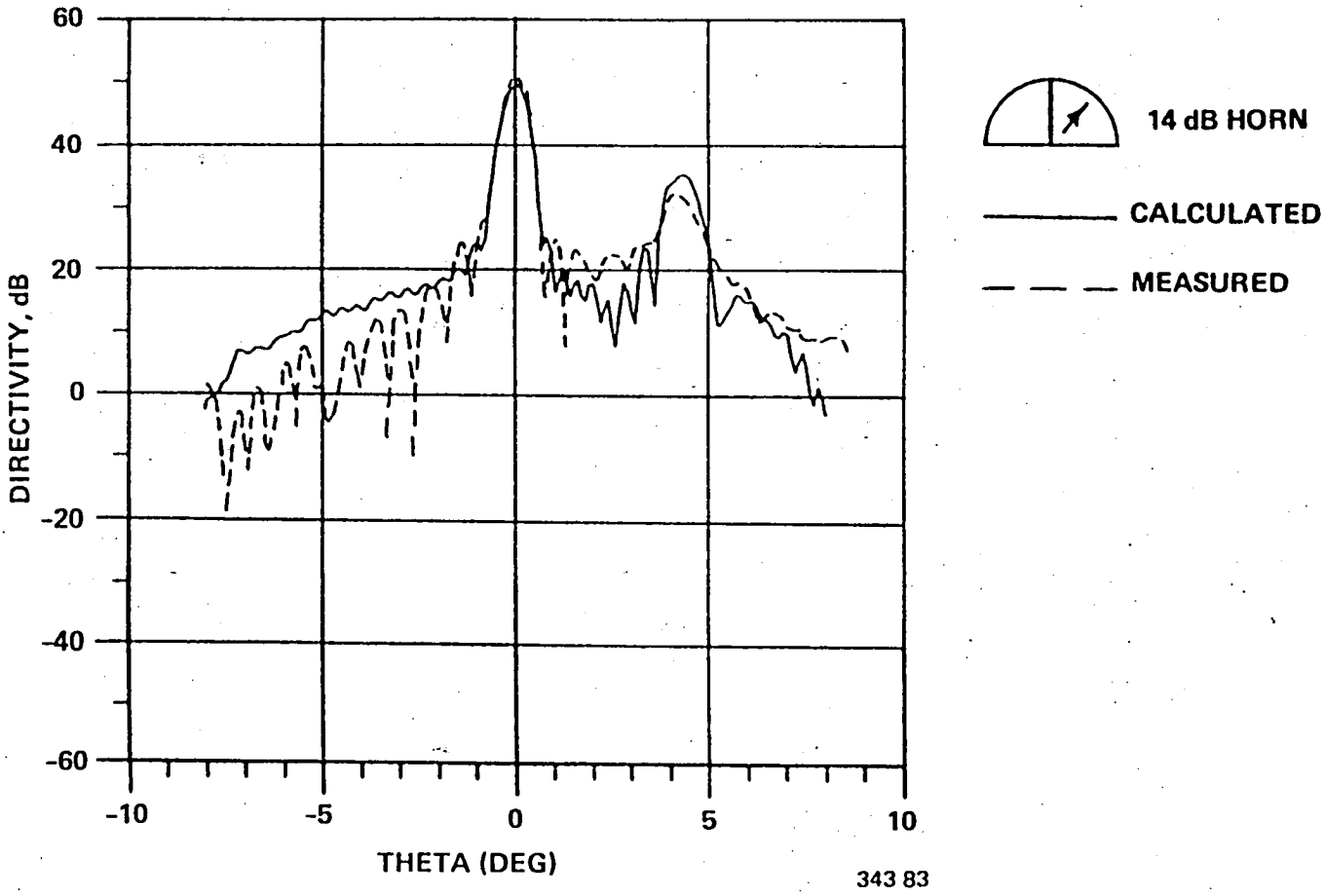

Figure 35. Dual Reflectors with 14 dB Horn Feed

(E- and H-Planes Asymmetric)

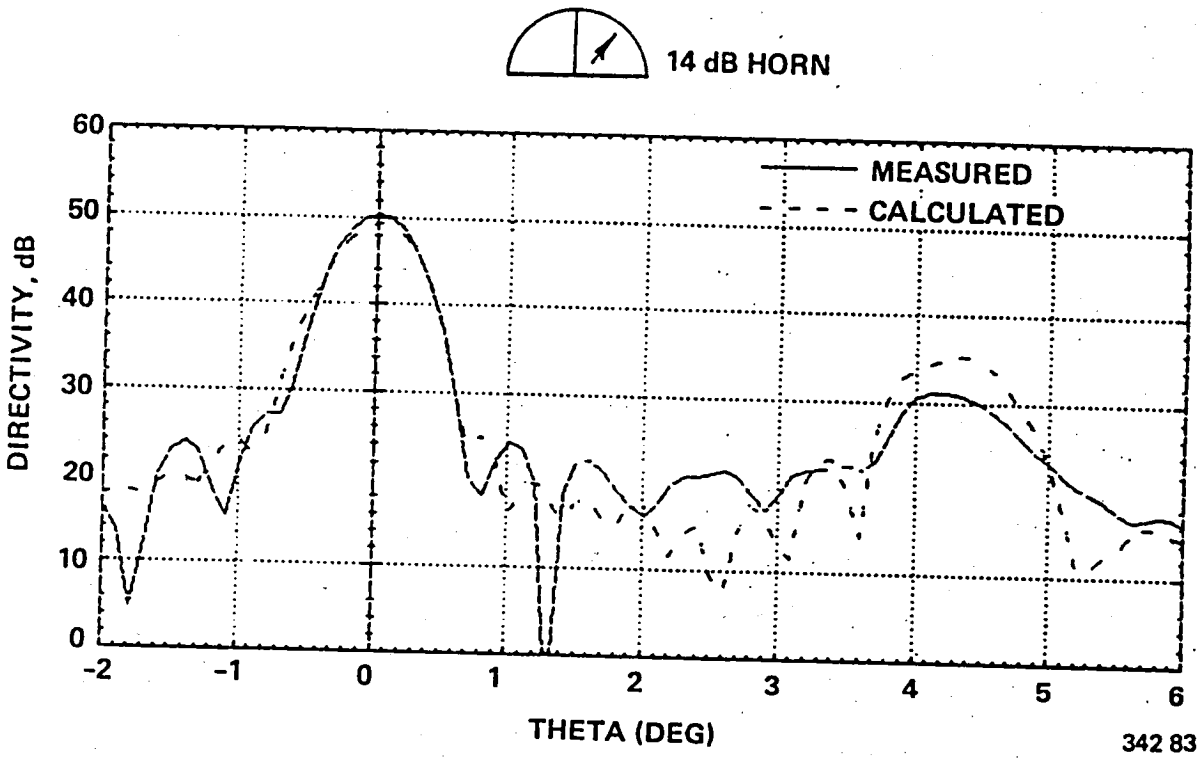

Figure 36. Dual Reflectors with 14 dB Horn Feed

(E- and H-Planes Asymmetric)

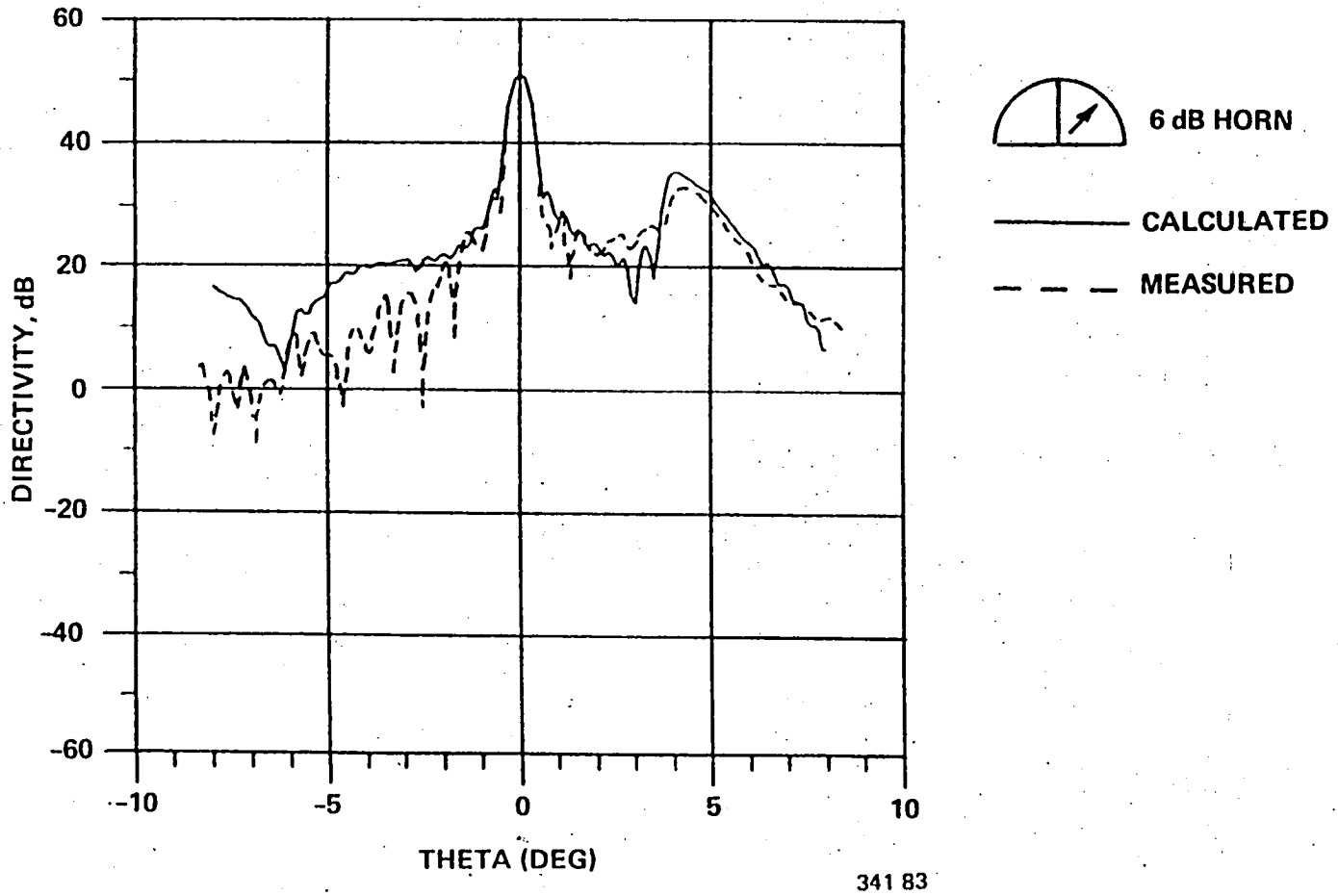

Figure 37. Dual Reflectors with 6 dB Horn Feed

(E- and H-Planes Symmetric)

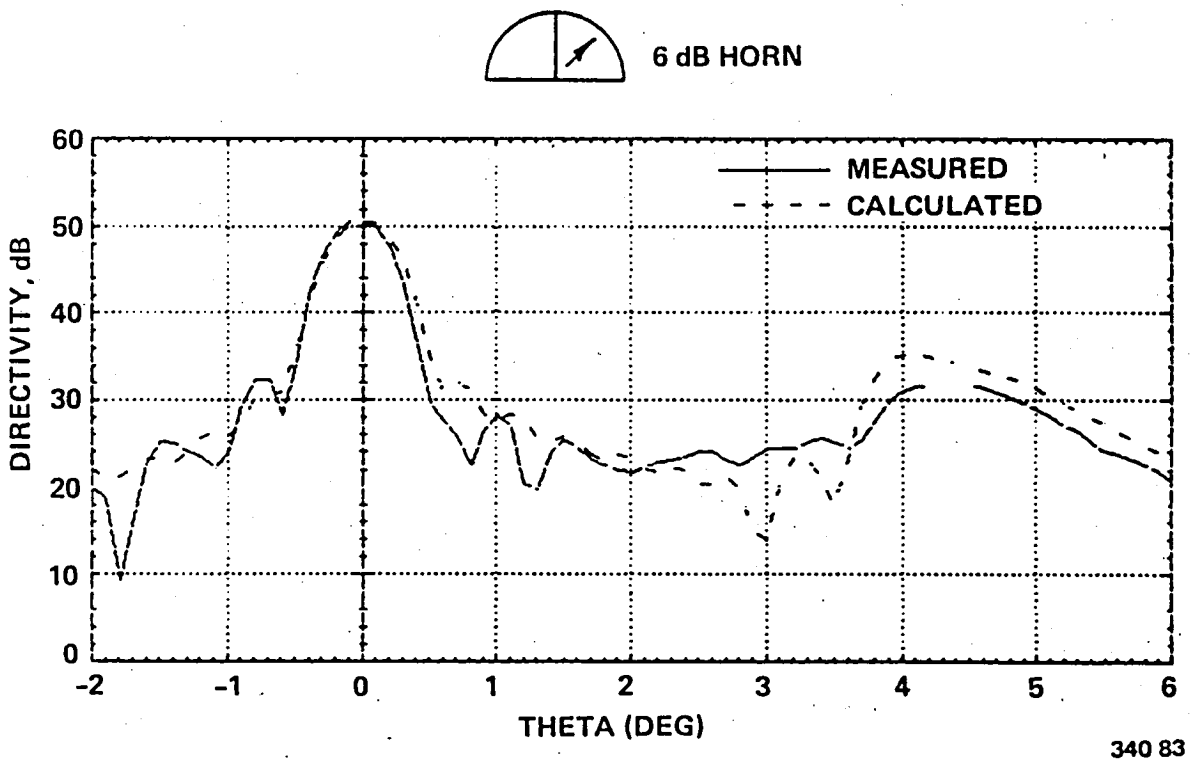

Figure 38. Dual Reflectors with 6 dB Horn Feed

(E- and H-Planes Symmetric)

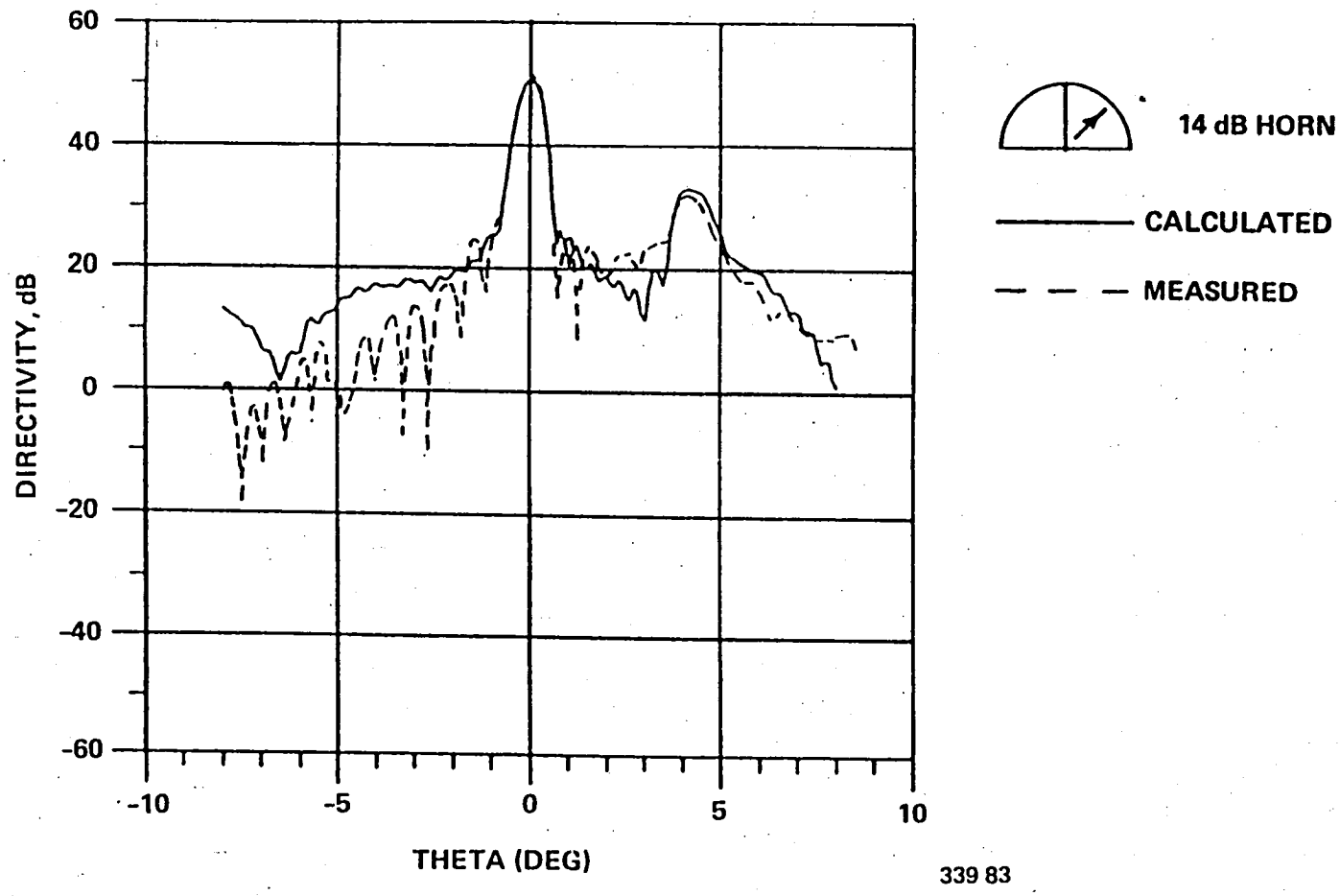

Figure 39. Dual Reflectors with 14 dB Horn Feed

(E- and H-Planes Symmetric)

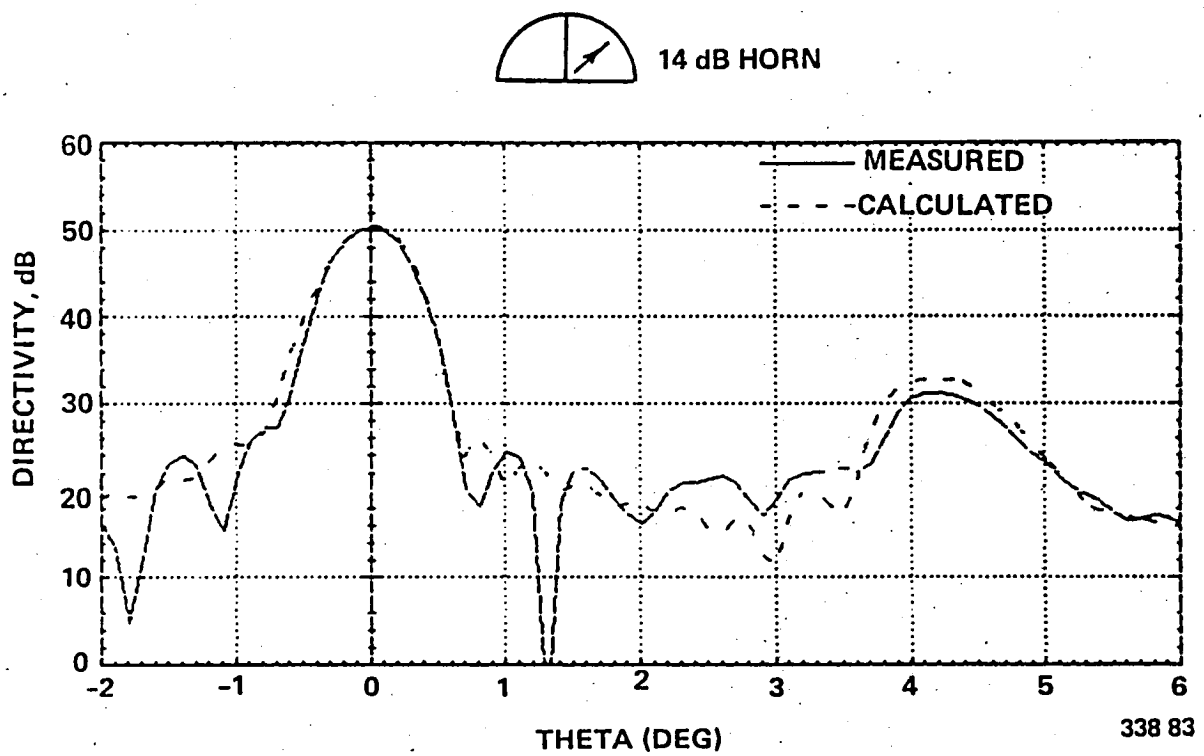

Figure 40. Dual Reflectors with 14 dB Horn Feed

(E- and H-Planes Symmetric)

Table I. Comparison of Measured and Calculated Results

		Peak Gain (dB)	Parasitic Side Lobe Level (Relative dB)
6 dB Horn	Measured	50.75	-15.90
	Calculated (E-H Asymmetric)	50.18	-14.15
	Calculated (E-H Symmetric)	50.76	-15.53
14 dB Horn	Measured	50.39	-19.10
	Calculated (E-H Asymmetric)	49.29	-13.97
	Calculated (E-H Symmetric)	50.49	-17.68

COMPARISON OF QUADRANT AND CIRCULAR APERTURES

In order to assess the effects of the nonstandard, quadrant reflectors, a comparison was made between the far-field patterns of circular aperture, offset paraboloids and quadrant reflectors. The 6 dB and 14 dB horns were again used as the feeds.

A front view of the physical geometry of the circular aperture is shown in Figure 41. The size of the reflectors was limited to that which would fit into the same space as the two quadrant reflectors. This resulted in a reflector radius of 42.75 inches and an axial point-to-reflector center offset of 52.66 inches. The focal distance remained at 137.7 inches, and hence, the parent paraboloid of both the circular and quadrant reflectors is the same. The criterion of fitting the reflector into equal space did result in a significant reduction in surface area.

The computer far-field patterns for the 6 dB and 14 dB horns are given in Figure 42 and Figure 43 where both the circular and quad aperture reflector geometries were used. From these results there are several observations that can be made: (1) the circular apertures produce a smaller gain due to the smaller scattering surface area, but the peaks and nulls of this pattern are well defined, indicating little phase error. In the region of the parasitic lobe, the nulls tend to fill in due to the off-focus excitation of the parasitic reflector; (2) the ratio of the parasitic lobe to the main lobe is approximately the same, regardless of reflector shape; and (3) the pie shaped quad sectors produce a general increase in close-in and far-out side lobe levels that indicates scattered fields that are defocused. Since the phase center of the feed horn is exactly the same for both cases, this increase in side lobe level must be due to currents on the pie shaped reflectors that are outside of the normal conical feed pattern projections on a offset parabola.

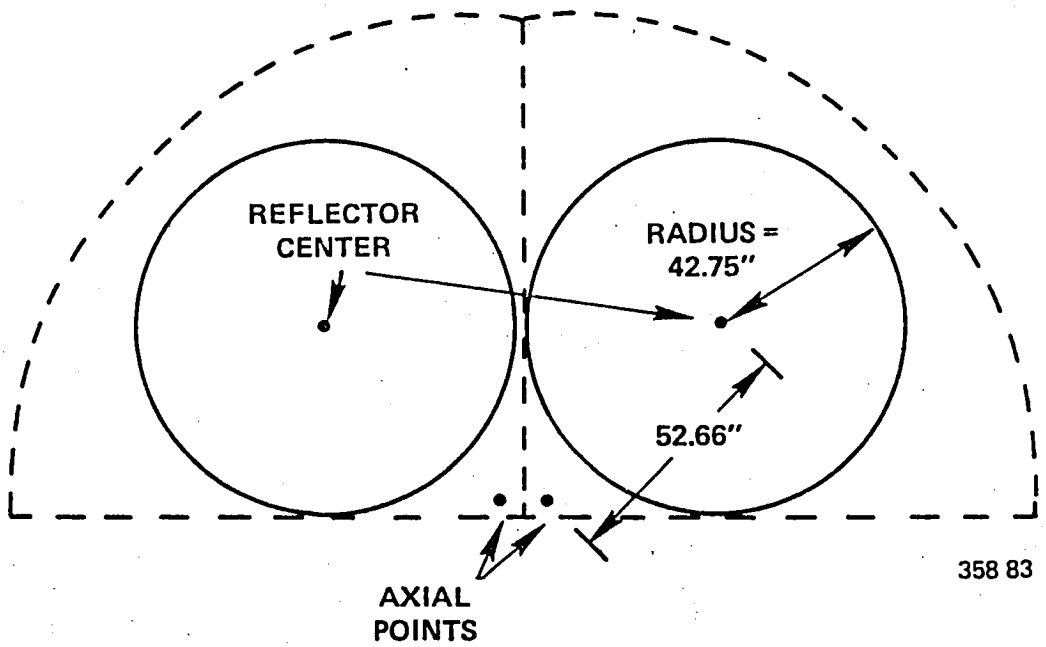

Figure 41. Circular Aperture, Offset Reflector Configuration

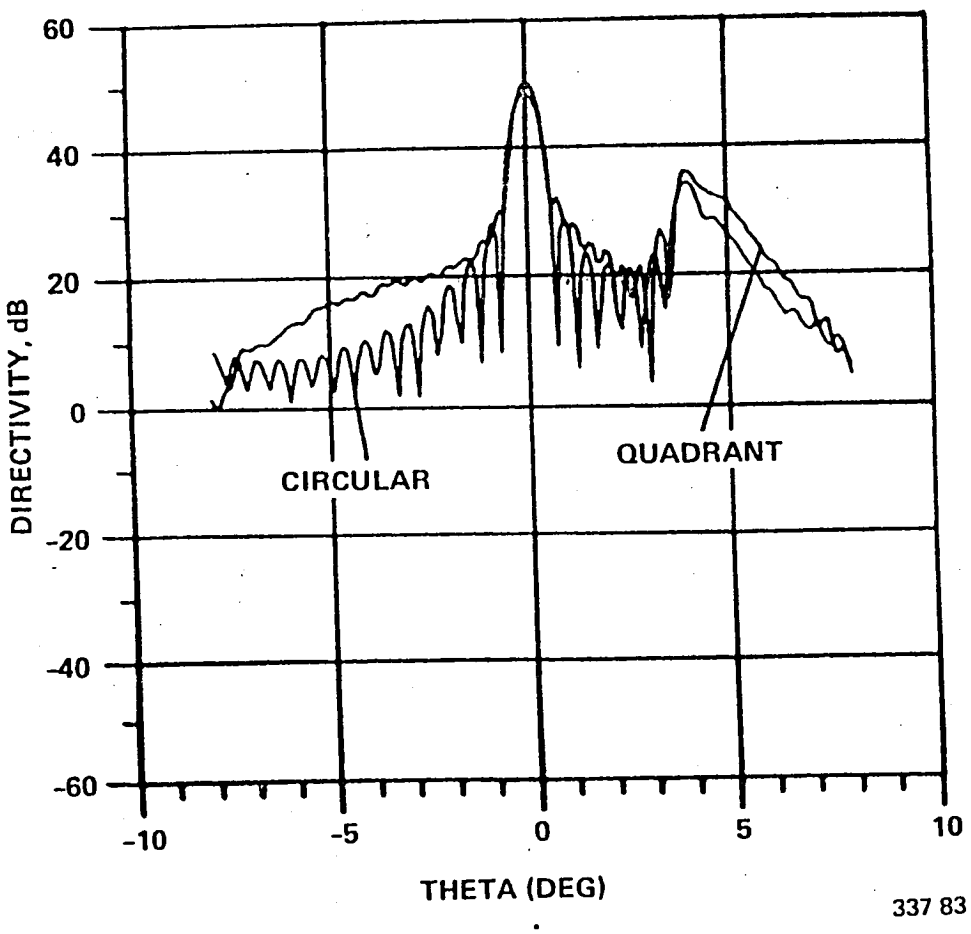

Figure 42. Comparison of Circular and Quadrant

Dual Reflector with 6 dB Horn Feed

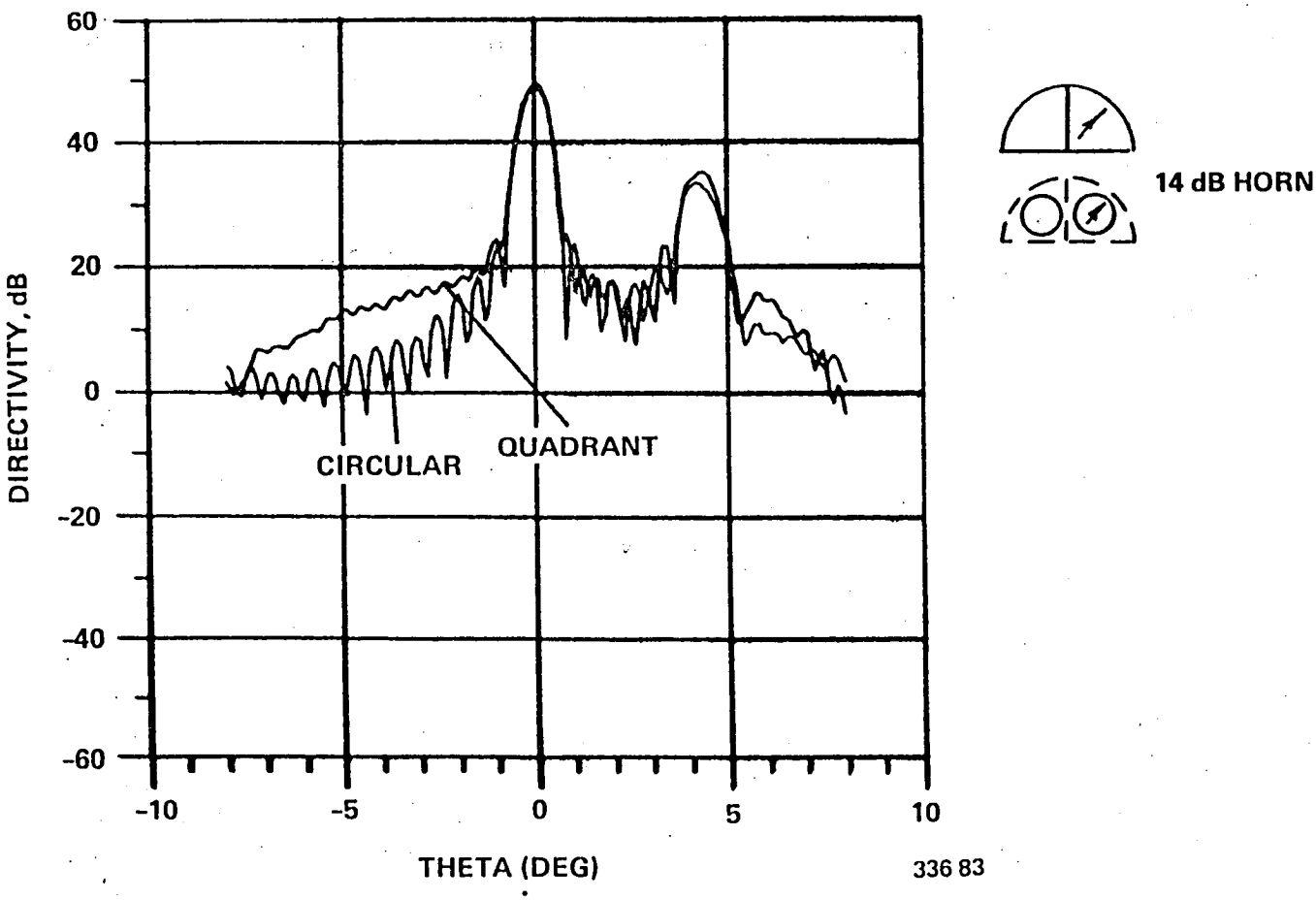

Figure 43. Comparison of Circular and Quadrant

Dual Reflector with 14 dB Horn Feed

DISCUSSION OF MEASURED RASTER SCAN CONTOUR PLOTS

In order to analyze the detailed three-dimensional scatter pattern characteristics of the quad aperture reflector fed by the 6 dB and 14dB pyramidal horns, contour plots were made using the digitized raster scan data. These measured contour plots are given in Figures 44 through 53. It is noted that due to the possible ±0.05 degree angular position measurement error, these plots may occasionally exhibit a small discontinuity. No attempt was made to smooth the data prior to applying the contour algorithm. Also note that the center of the main beam was always pointed to 0,0, regardless of the feed scan angle.

The measurements for the single quad aperture where the 6 dB feed is scanned 0.0 and 4.5 inches (≈3 BW) in the aperture plane are given in Figures 44 and 45. The basic change in the pattern is at the -20 dB contour level which spreads in angular width in the plane of scan. This is a typical behavior of scanned feed reflectors. The measurements of the 6 dB horn illuminating the two quad apertures with orthogonal linear polarizations are given in Figures 46 and 47. It should be noted that the parasitic lobe is primarily confined to the azimuth plane and has a quasi-elliptical shape which is narrower than the contour at the corresponding power level. This behavior is quite general, regardless of edge taper, as demonstrated later. The change in polarization relative to the sector edge does not seem to affect the overall amplitude and shape of the reflector scattered field, and indicates a lack of sensitivity to that parameter.

The contoured measurements of the 14 dB horn feeding the single quad aperture at 0, 4.5, and 6.5 inches scan are given in Figures 48 through 50. The gain change as a function of scan is small (0.45 dB for 5 BW scan) which

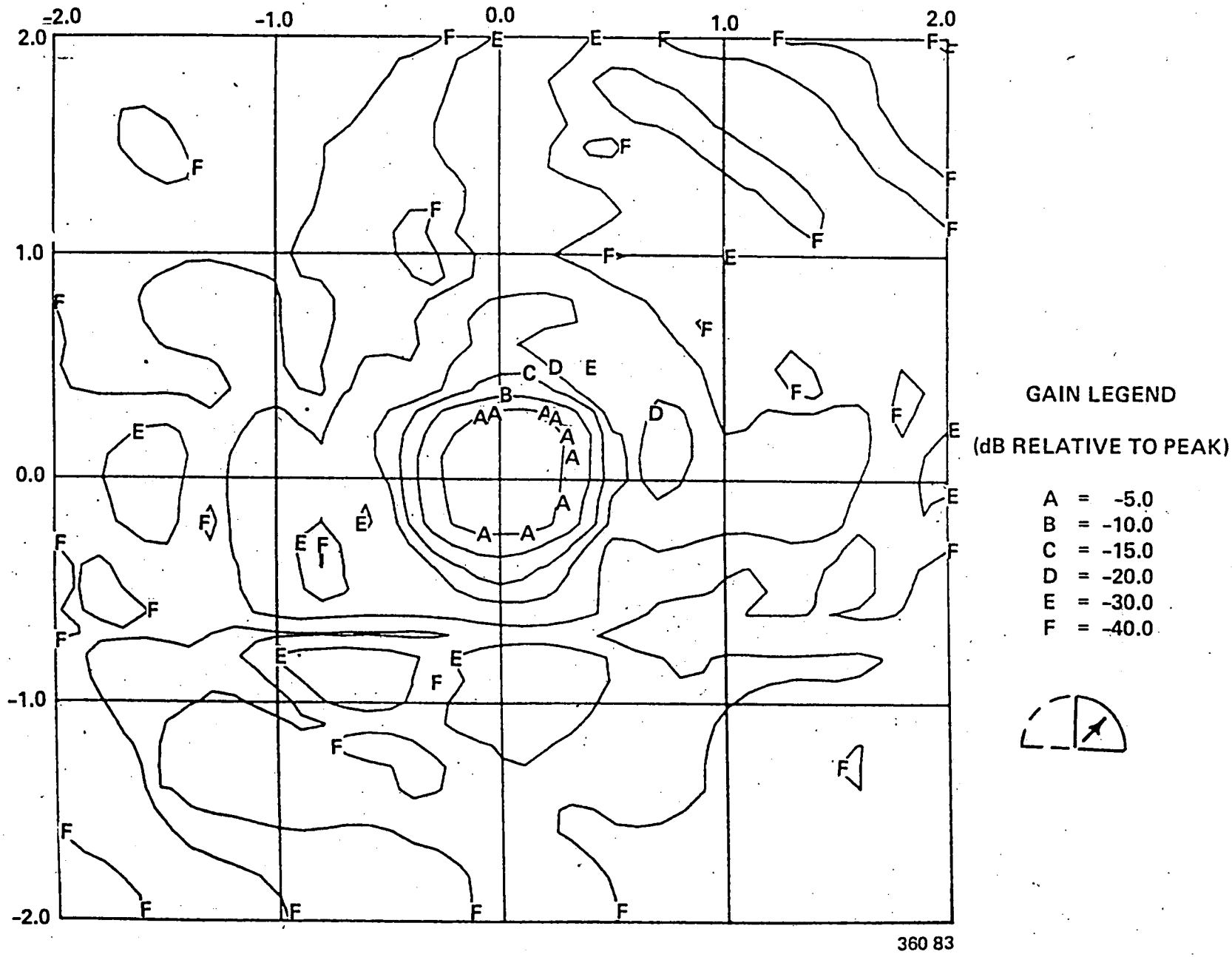

Figure 44. 6 dB Horn, 0.0" Scan

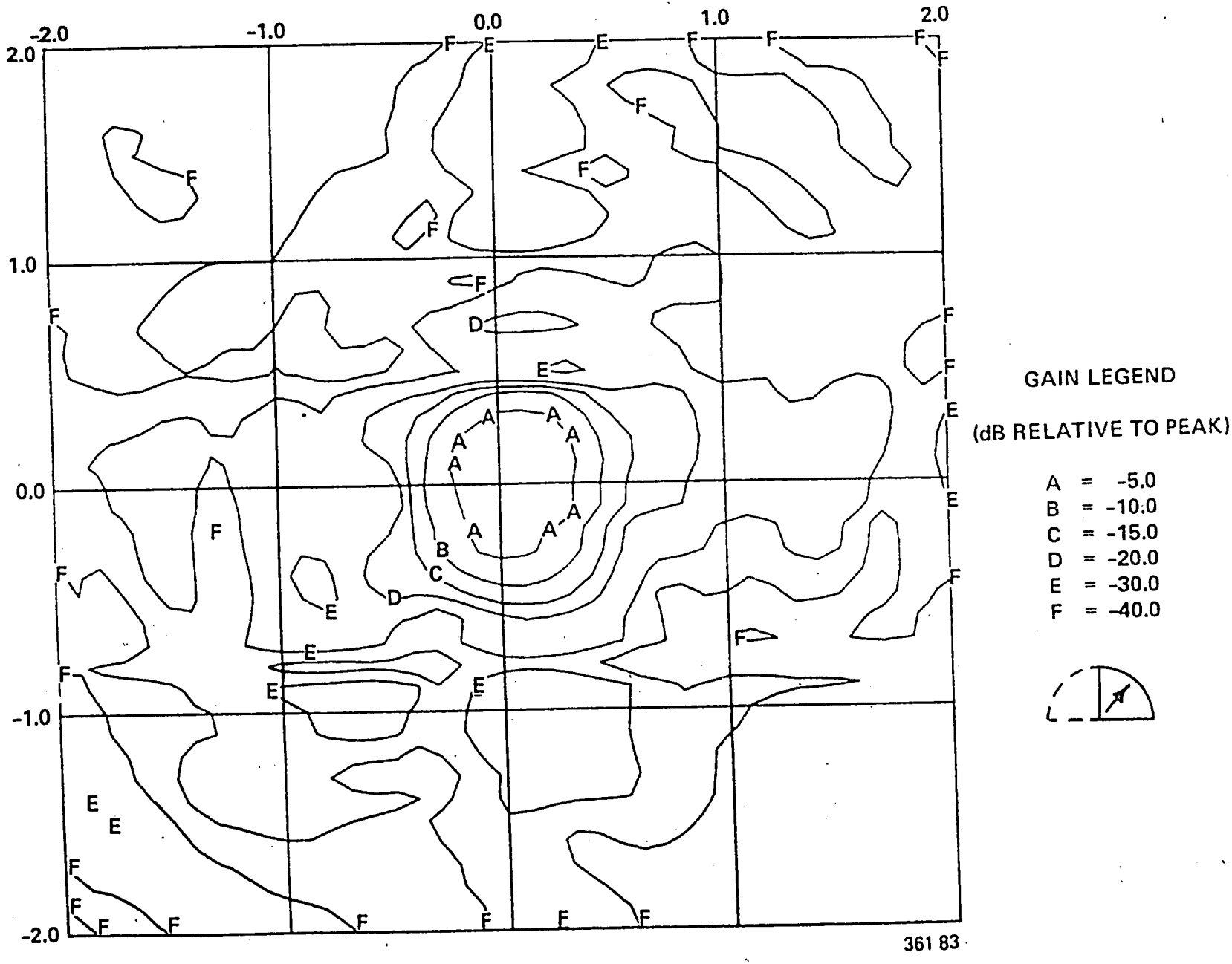

Figure 45. 6 dB Horn, 4.5" Scan

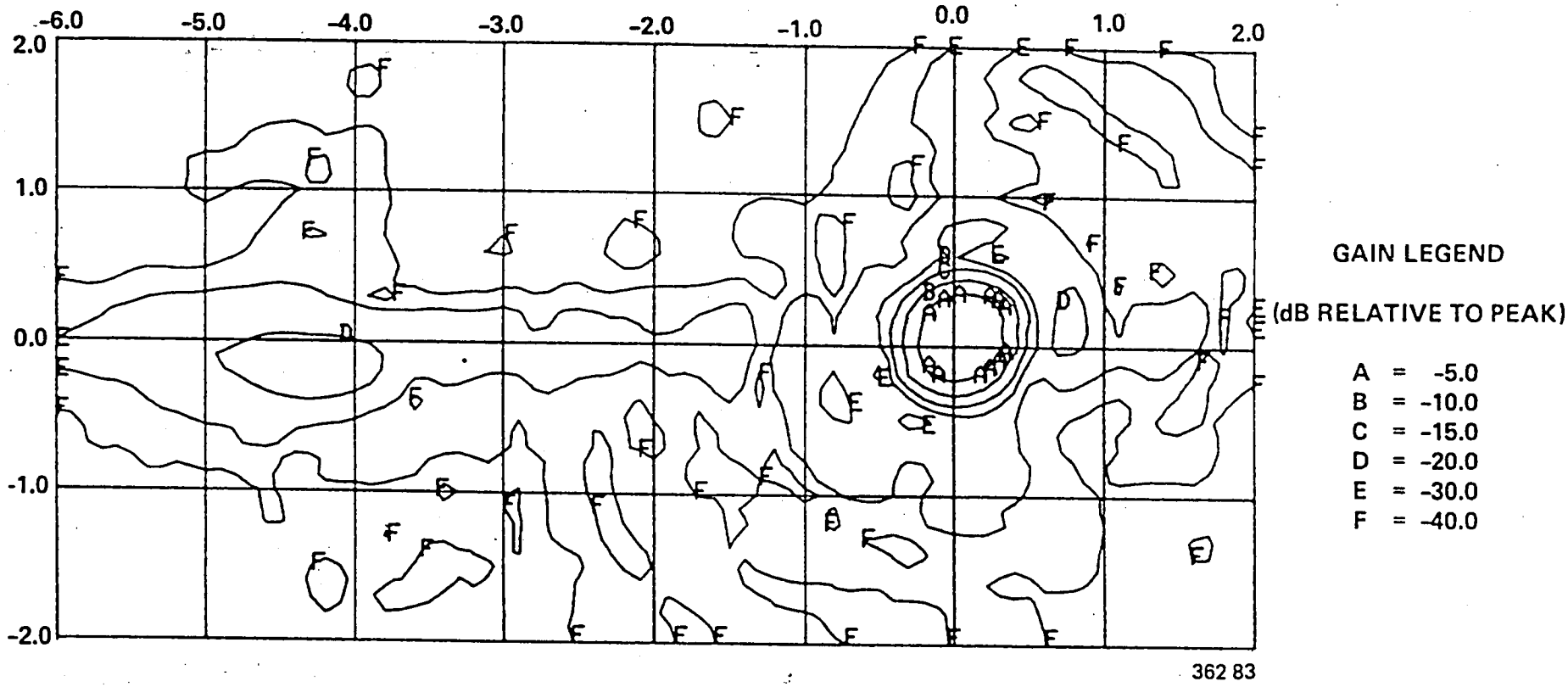

Figure 46. 6 dB Horn, 0.0" Scan

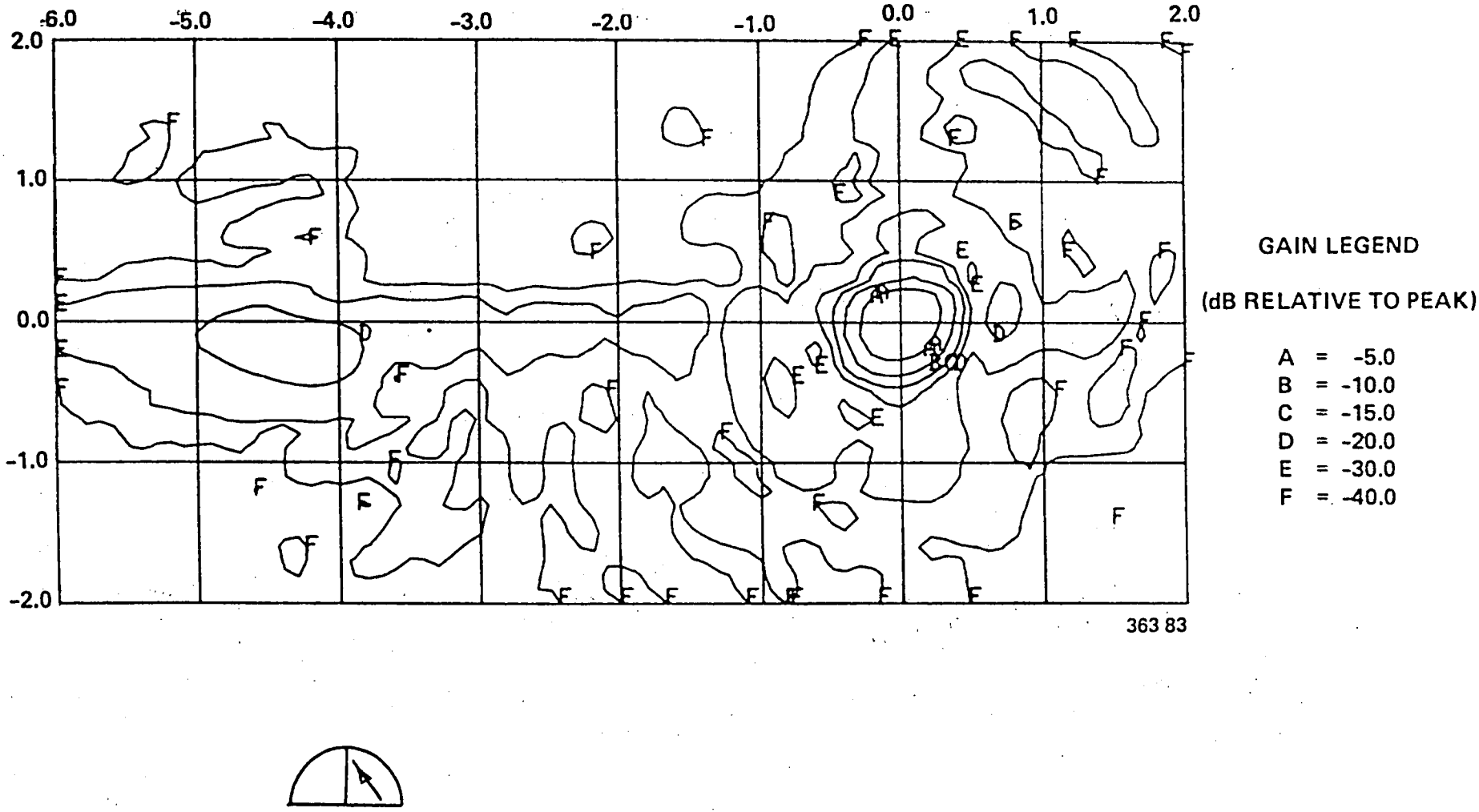

Figure 47. 6 dB Horn, 0.0" Scan

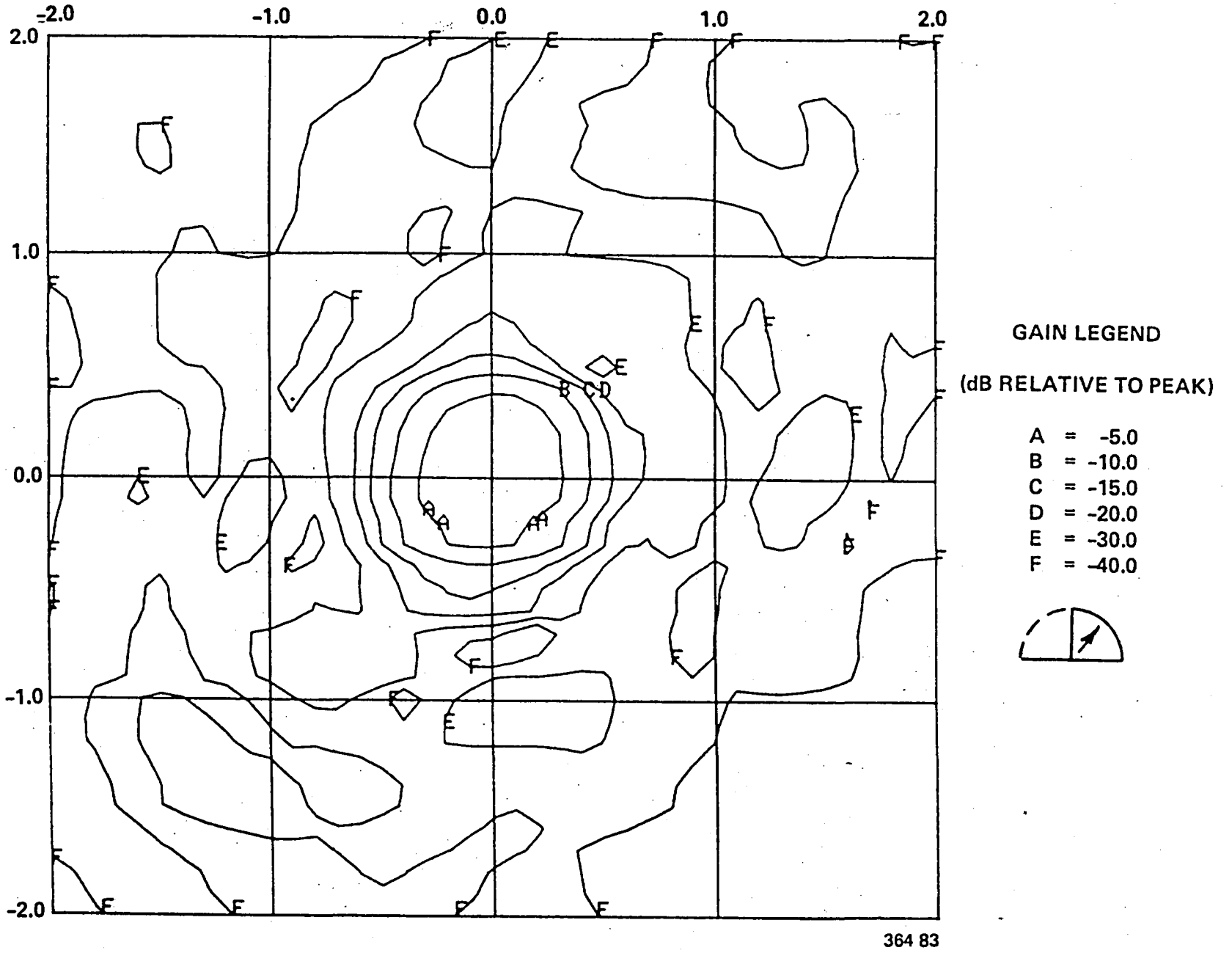

Figure 48. 14-dB Horn, 0.0" Scan

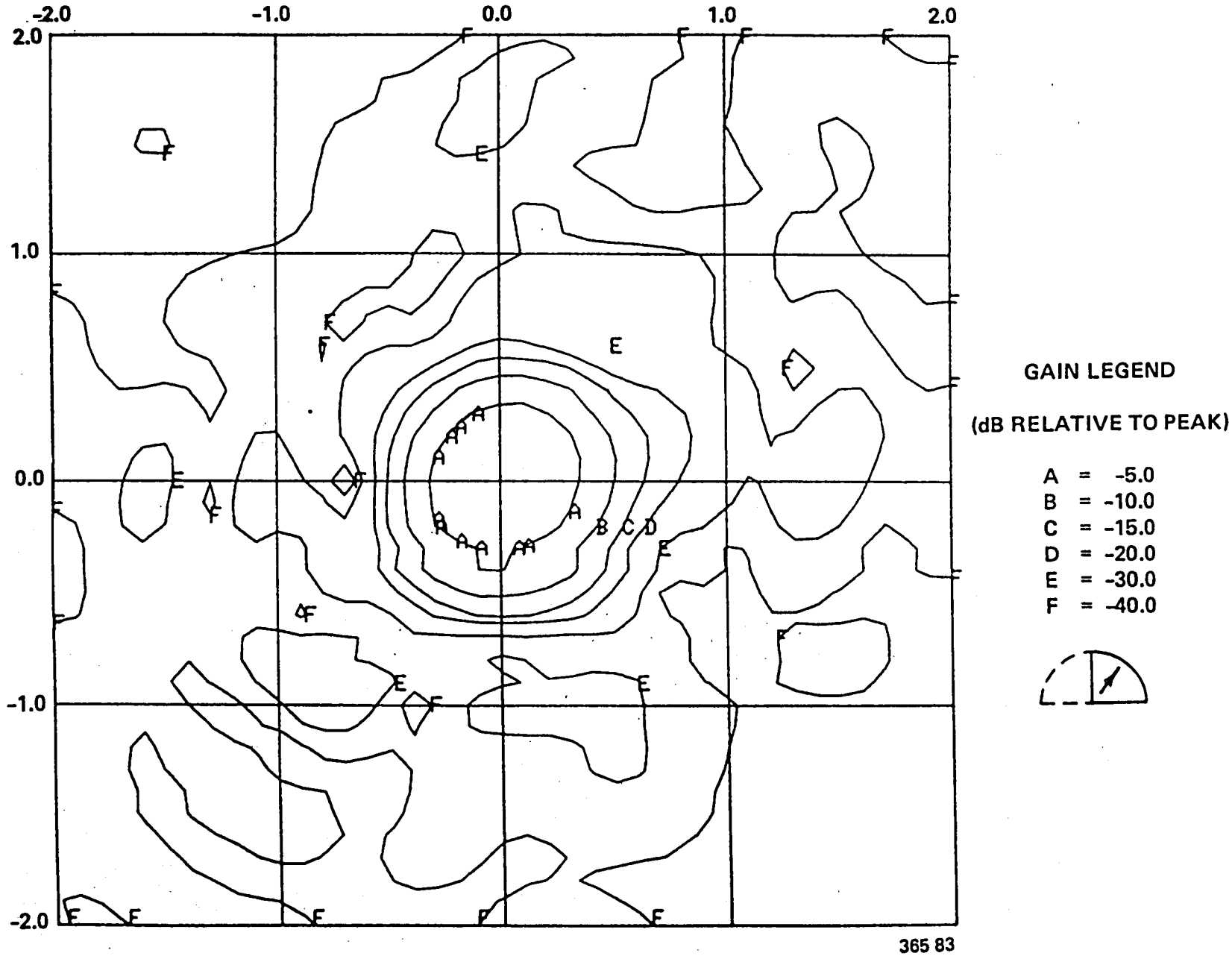

Figure 49. 14 dB Horn, 4.5" Scan

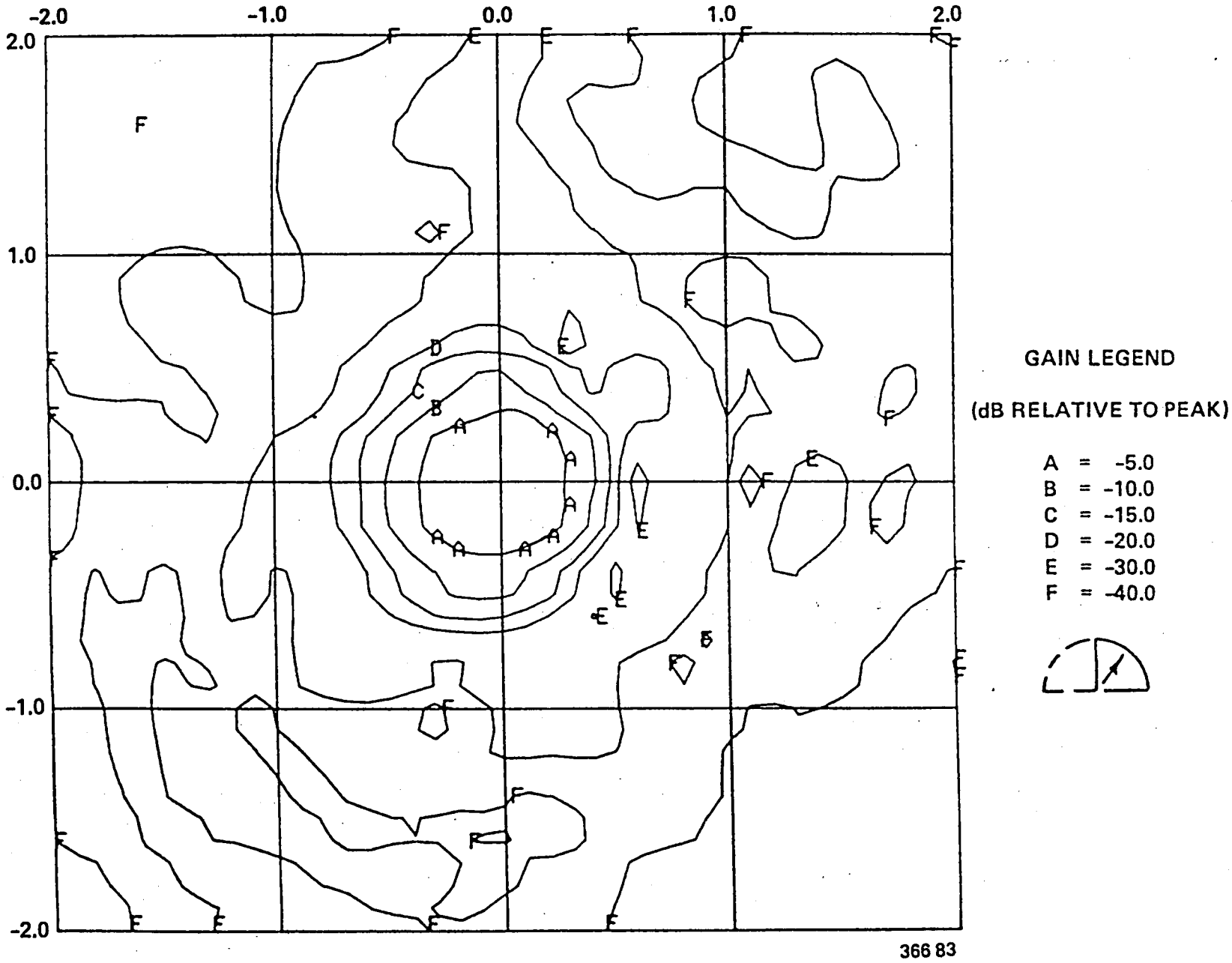

Figure 50. 14 dB Horn, 6.5" Scan

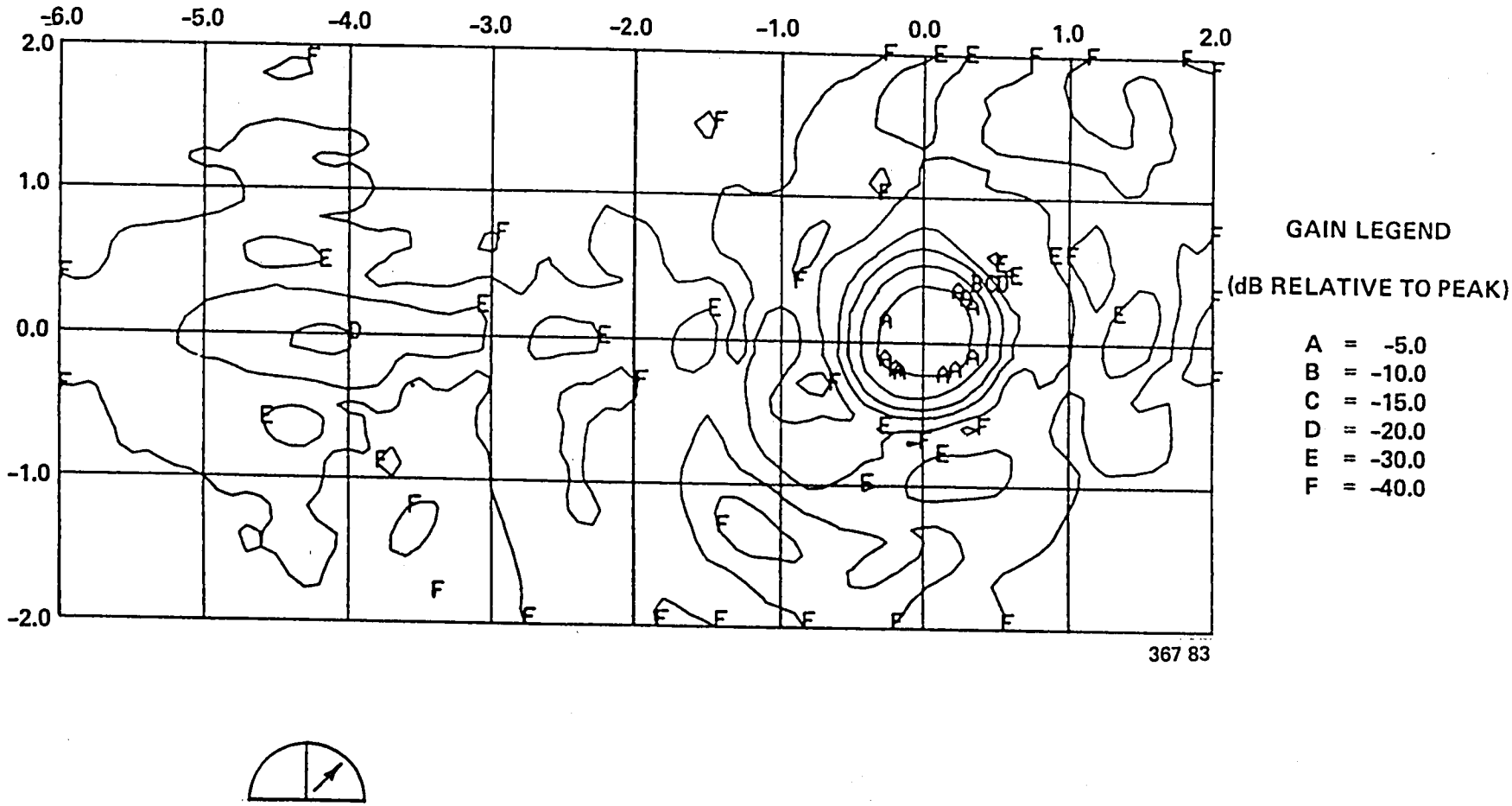

Figure 51. 14 dB Horn, 0.0" Scan

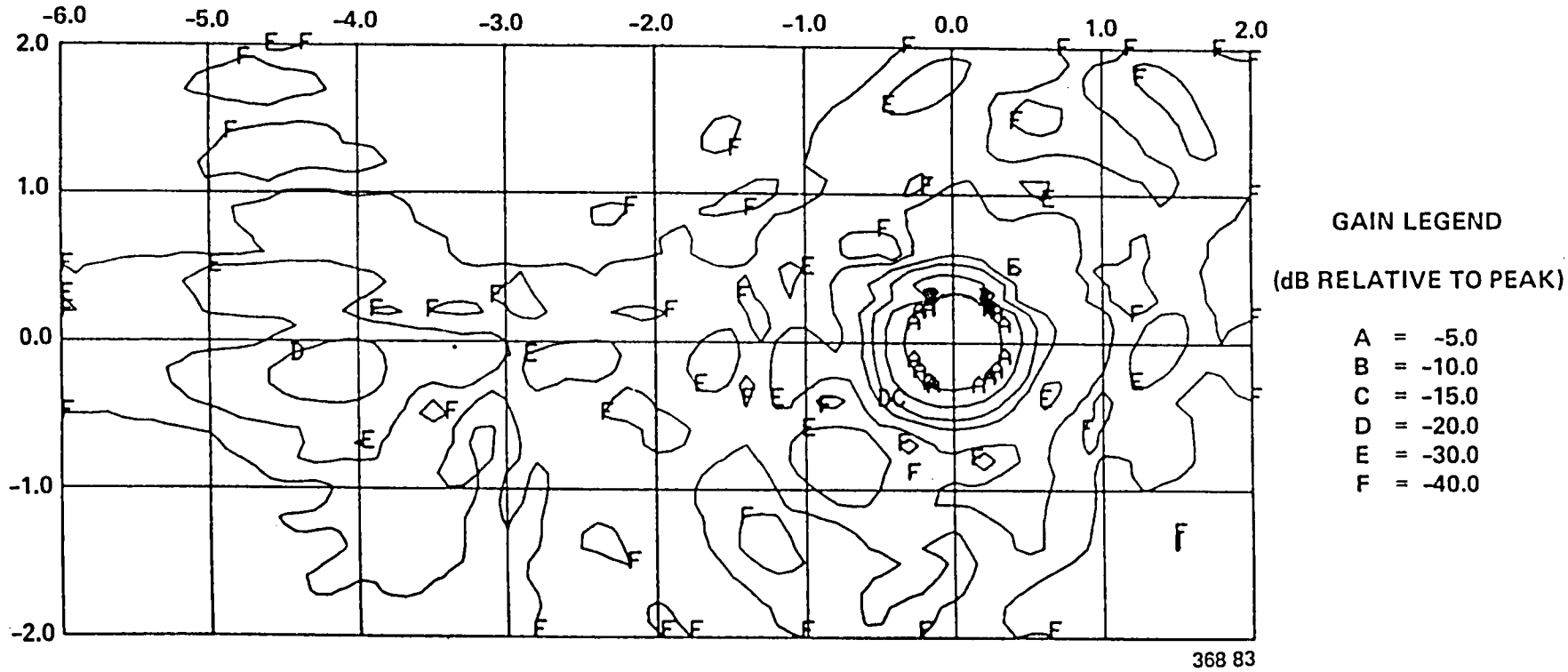

Figure 52. 14 dB Horn, 0.0" Scan

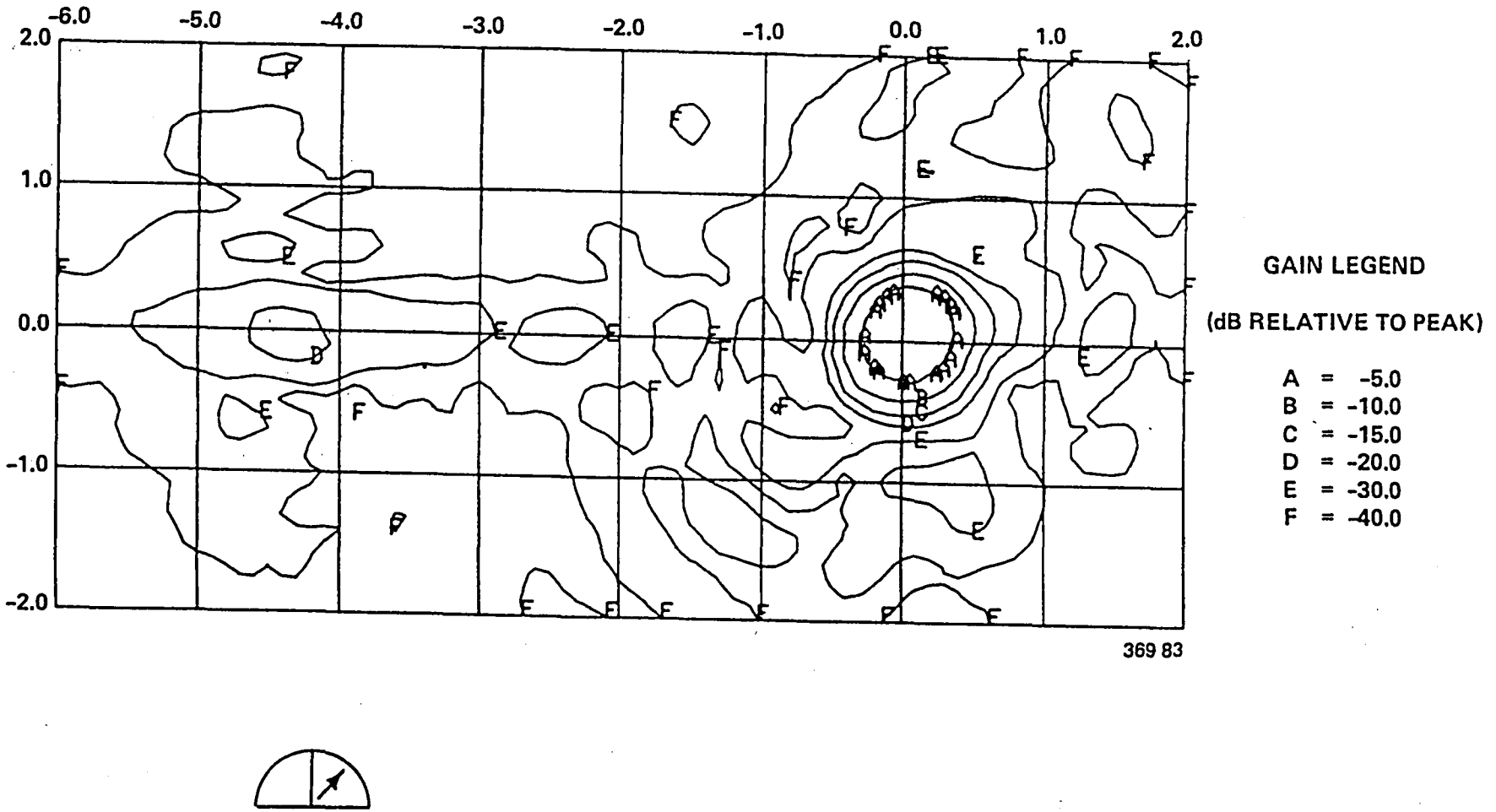

Figure 53. 14 dB Horn, 4.5" Scan

is expected of a long focal length reflector system. The general broadening of the pattern at the -20 dB level is evident. Figures 51 through 53 present orthogonal polarization and scan feed data for dual quad reflectors with the 14 dB excitation. The parasitic scattering lobe is very narrow in this instance, but appears to have a similar amplitude and location relative to the main lobe for the three cases considered.

The significant conclusion that is drawn from inspecting these data is that the major parasitic lobe, due to low-level feed radiation striking an adjacent reflector, is confined to a fairly narrow sector region about its peak value. Precise experimental determination of the magnitude of this lobe will require exceptional angular resolution for the antenna pedestal beyond the normal capability in standard antenna ranges, particularly for large reflectors. The result of this angular sensitivity is that precision agreement with calculations will be difficult.

USE OF CORRUGATED HORNS AS FEED ELEMENTS

Earlier results have shown that a more sophisticated feed is necessary to improve the antenna performance, especially in the area of parasitic side lobe level. A feed which (1) has a symmetric pattern and (2) a high beam efficiency, in the area of the main quadrant should be a step in the right direction toward accomplishing these goals.

Our methodology in approaching this problem was to choose an element with a symmetric pattern and determine what subset of designs for this feed element gave satisfactory beam efficiency.

The first element type to be included in this feed study was the corrugated conical horn. The model for his horn is shown in Figure 54. Corrugated horns with $\Delta < \sim 0.4$ (see Figure 54) are sometimes referred to as "narrowband horns"; their performance depends primarily on aperture size.

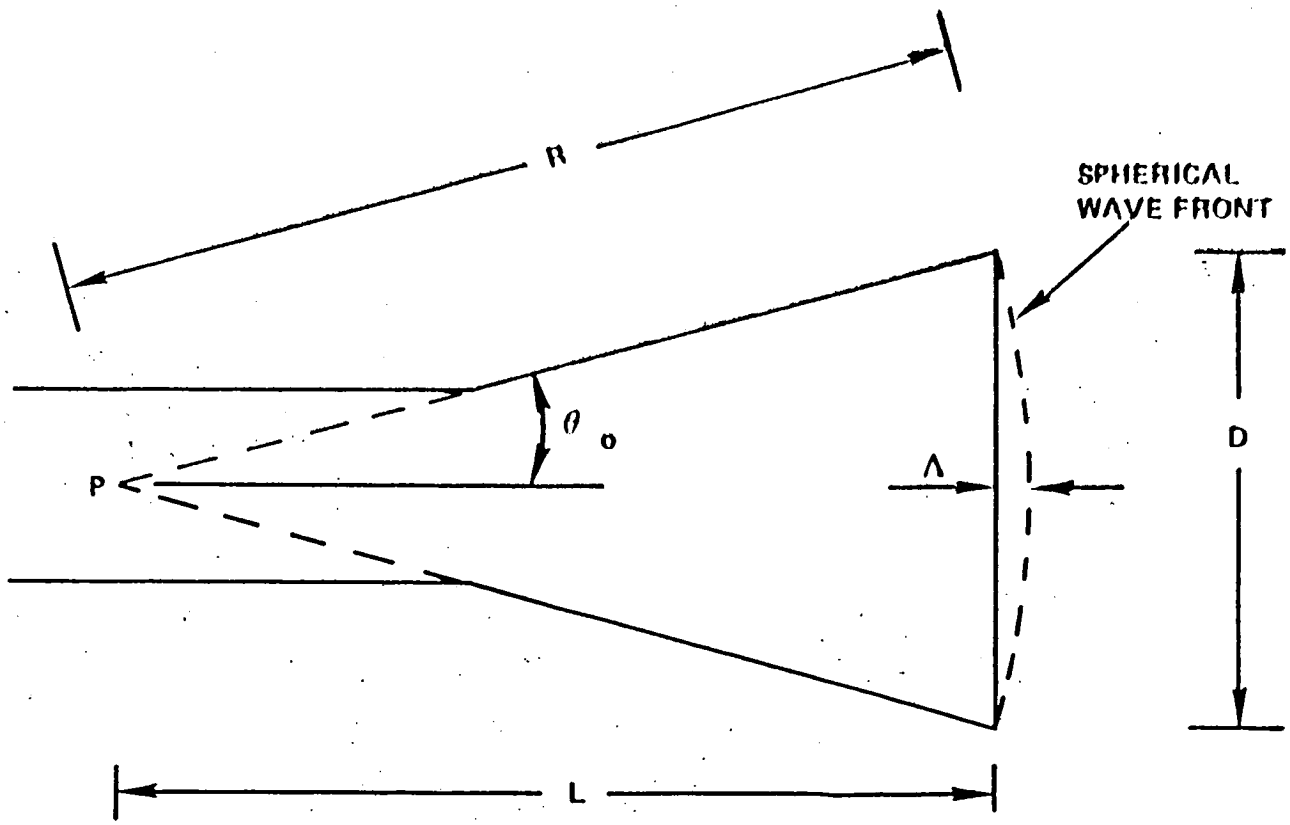

P = PHASE CENTER
D = APERTURE DIAMETER
L = LENGTH OF HORN (PHASE CENTER TO APERTURE)
R = RADIUS (PHASE CENTER TO SPHERICAL WAVE FRONT IN APERTURE)
θ_o = FLARE ANGLE OF HORN
Δ = MAXIMUM PHASE ERROR IN APERTURE (IN WAVELENGTHS)

370 83

Figure 54. Corrugated Conical Horn Model

Those horns with $\Delta > \sim 0.75$ can be called "wideband horns" or "scalar horns." Performance of these horns depends mainly on flare angle. In our investigation, we did not restrict ourselves to corrugated horns of any type, although the majority of those horns chosen for final study clearly fall in the narrowband region. From past experience, it has been found that a good aperture field model is a cosine amplitude variation, and quadratic phase due to horn length and flare. An aperture integration similar to that shown for the pyramidal horn was used to calculate the patterns.

As feed beam efficiency goes up (measured at the edge of the reflector, ~21°), less energy should spill onto adjacent quadrants, with an accompanying drop in parasitic side lobe level. As a first step, beam efficiency was computed and plotted as a function of aperture diameter, along lines of constant horn length. This graph, given in Figure 55, shows that as diameter gets larger (in wavelengths), beam efficiency rises due to narrowing of the main beam. However, as the diameter continues to increase, beam efficiency falls, due to larger phase error across the aperture. The point at which this drop begins can be seen to be a function of horn length.

Some preliminary far-field calculations showed that higher and higher beam efficiencies did not necessarily result in lower parasitic side lobe level. A plausible explanation for this is that beyond some point, increasing beam efficiency is largely due to the inclusion of side lobe energy in the angular region over which beam efficiency is calculated. This "out-of-phase" energy seems to degrade peak gain levels faster than the diminishing spillover decreases the parasitic side lobe level.

This discovery led to a closer study of the beam efficiency question. It was determined to restrict the investigation to those horn designs which had more than some minimum beam efficiency, but which illuminated the reflector region with main beam energy only. In effect, this limits the possible

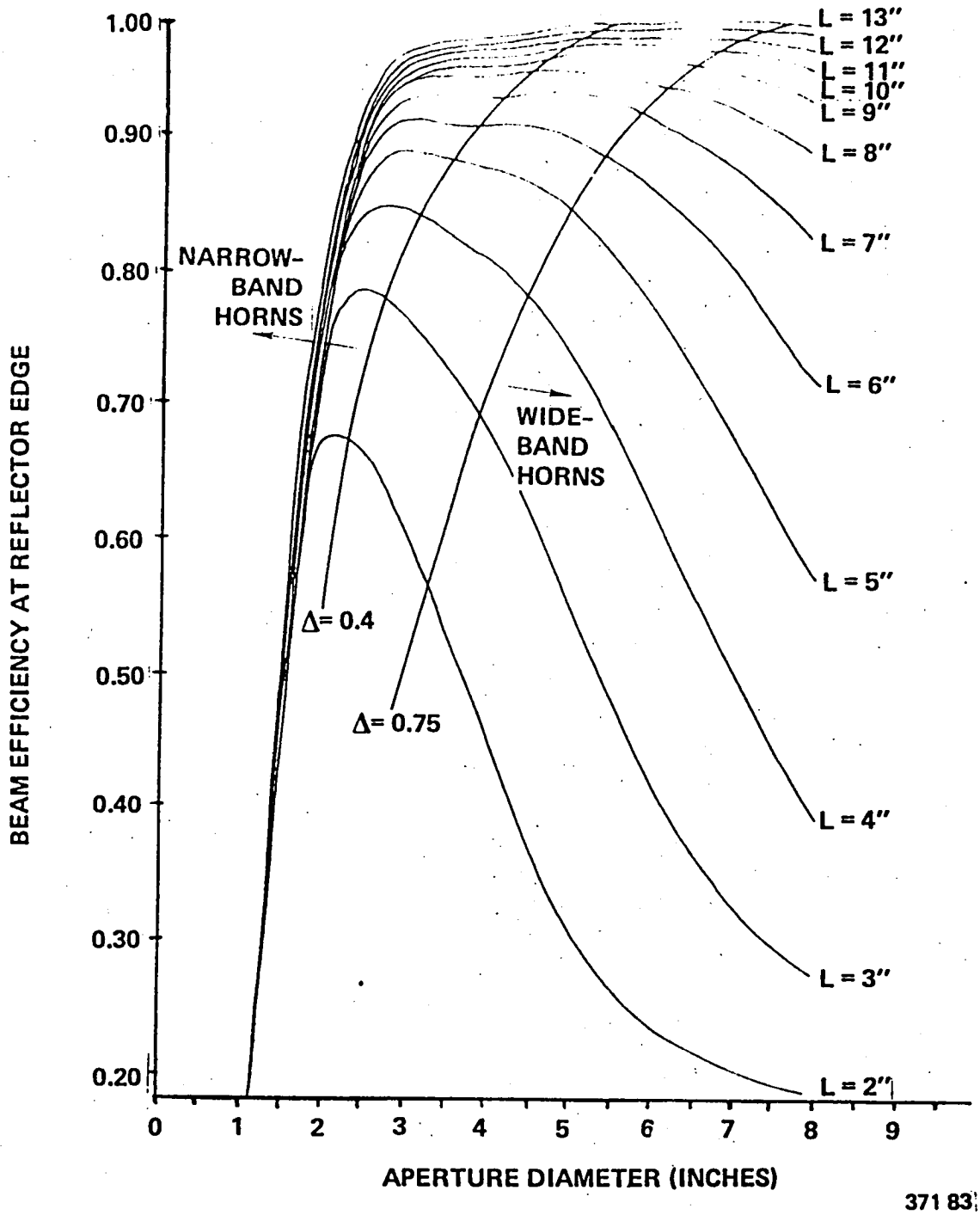

Figure 55. Beam Efficiency Versus Aperture Diameter

candidates to those whose primary pattern has low side lobes and the first null in the 18°-22° region.

The region of investigation was bounded by calculating primary patterns for horns with $\Delta = 0.0$. These designs give the best efficiency for a given diameter although they are physically unrealizable. The aperture diameters that are of interest turn out to be from 2.0 inches (2.54 λ) to 5.0 inches (6.35 λ). As aperture phase error increases, beam efficiency at a given diameter should degrade. Figure 56 bears this out, which shows beam efficiency plotted against aperture diameter, plotted in this case along line of constant Δ. Of the designs available in this region, twenty were chosen for further study.

These twenty corrugated horn patterns were used as input to the reflector code in order to assess their effect on parasitic side lobe level. The results of the computer analysis are presented in tabular form, Table II, and graphical form, Figure 57, where relative parasitic side lobe level is plotted as a function of aperture diameter along lines of constant phase error. Some typical primary and secondary patterns are given in Figures 58 through 61.

Two trends are evident and should be noted. Firstly, parasitic side lobe level increases for a given diameter as aperture phase error increases. This should be expected, as phase error quickly degrades peak gain performance. Secondly, as aperture diameter increases, side lobe level falls (for a given Δ). This is probably due to increasing beam efficiency. However, the curves appear to be leveling off for some of the smaller phase errors. This seems to support our earlier findings that at some point, increasing aperture size no longer results in lower parasitic side lobe level. At any rate, the results indicate that few, if any, of these corrugated horn designs are satisfactory.

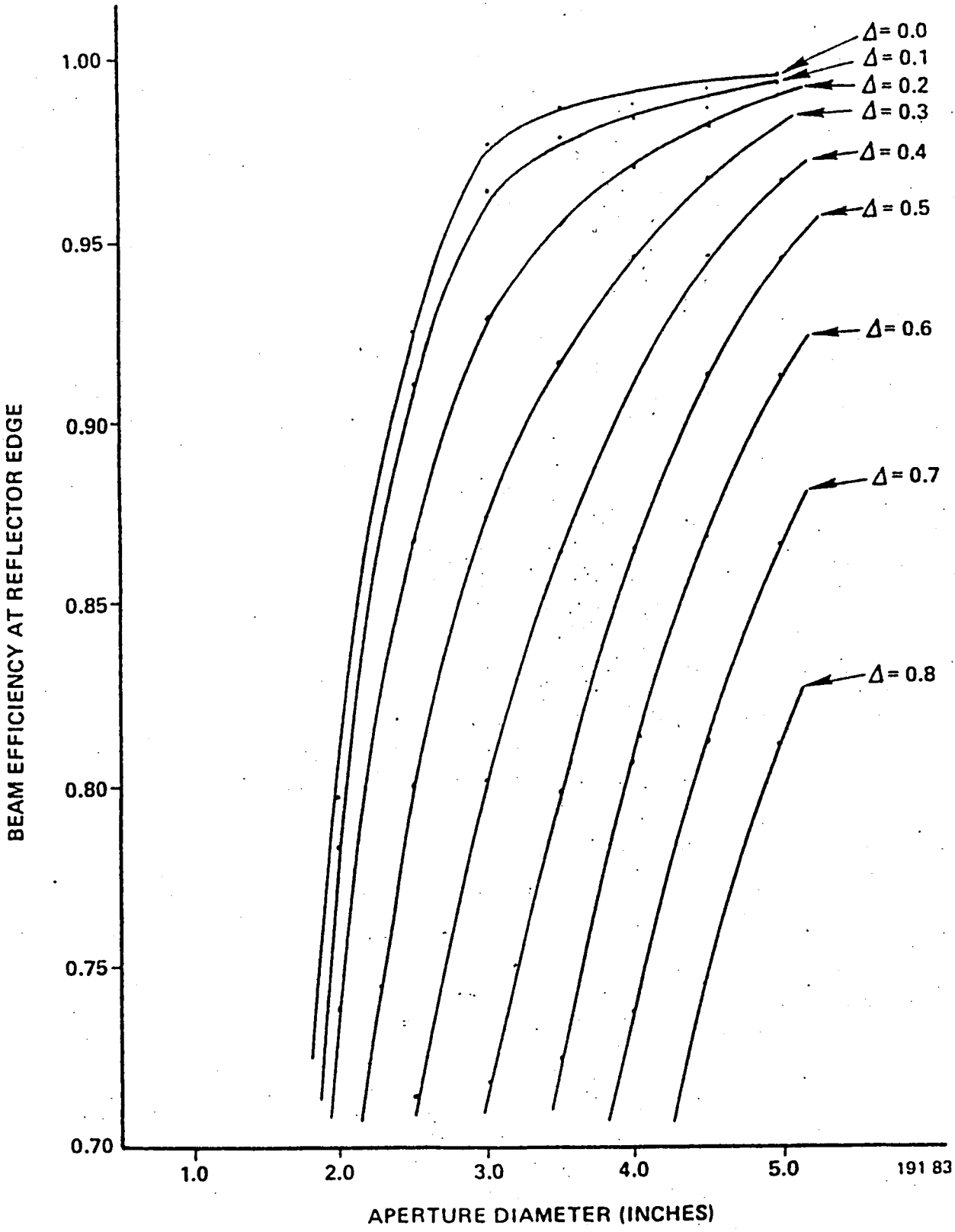

Figure 56. Beam Efficiency Versus Aperture Diameter

Table II. Corrugated Horn Feeds - Comparative Test Results

Phase Error (Wavelengths)	Aperture Diameter (Inches)	Aperture Diameter (Wavelengths)	Peak Gain (dB)	Parasitic Side Lobe Level (dB Relative) to Peak)
0.0	2.5	3.18	51.10	-19.72
0.0	3.0	3.81	50.73	-25.48
0.0	3.5	4.44	49.97	-28.35
0.0	4.0	5.08	48.96	-28.70
0.0	4.5	5.72	47.85	-28.87
0.1	2.5	3.18	51.03	-17.70
0.1	3.0	3.81	50.68	-21.61
0.1	3.5	4.44	49.93	-24.52
0.1	4.0	5.08	48.95	-25.58
0.1	4.5	5.72	47.88	-26.73
0.2	3.0	3.81	50.54	-18.28
0.2	3.5	4.44	49.86	-20.19
0.2	4.0	5.08	48.96	-21.67
0.2	4.5	5.72	48.00	-23.40
0.3	3.5	4.44	49.76	-17.09
0.3	4.0	5.08	49.00	-18.66
0.3	4.5	5.72	48.22	-20.51
0.4	4.0	5.08	49.04	-16.28
0.4	4.5	5.72	48.40	-18.06
0.5	4.5	5.72	48.48	-15.87

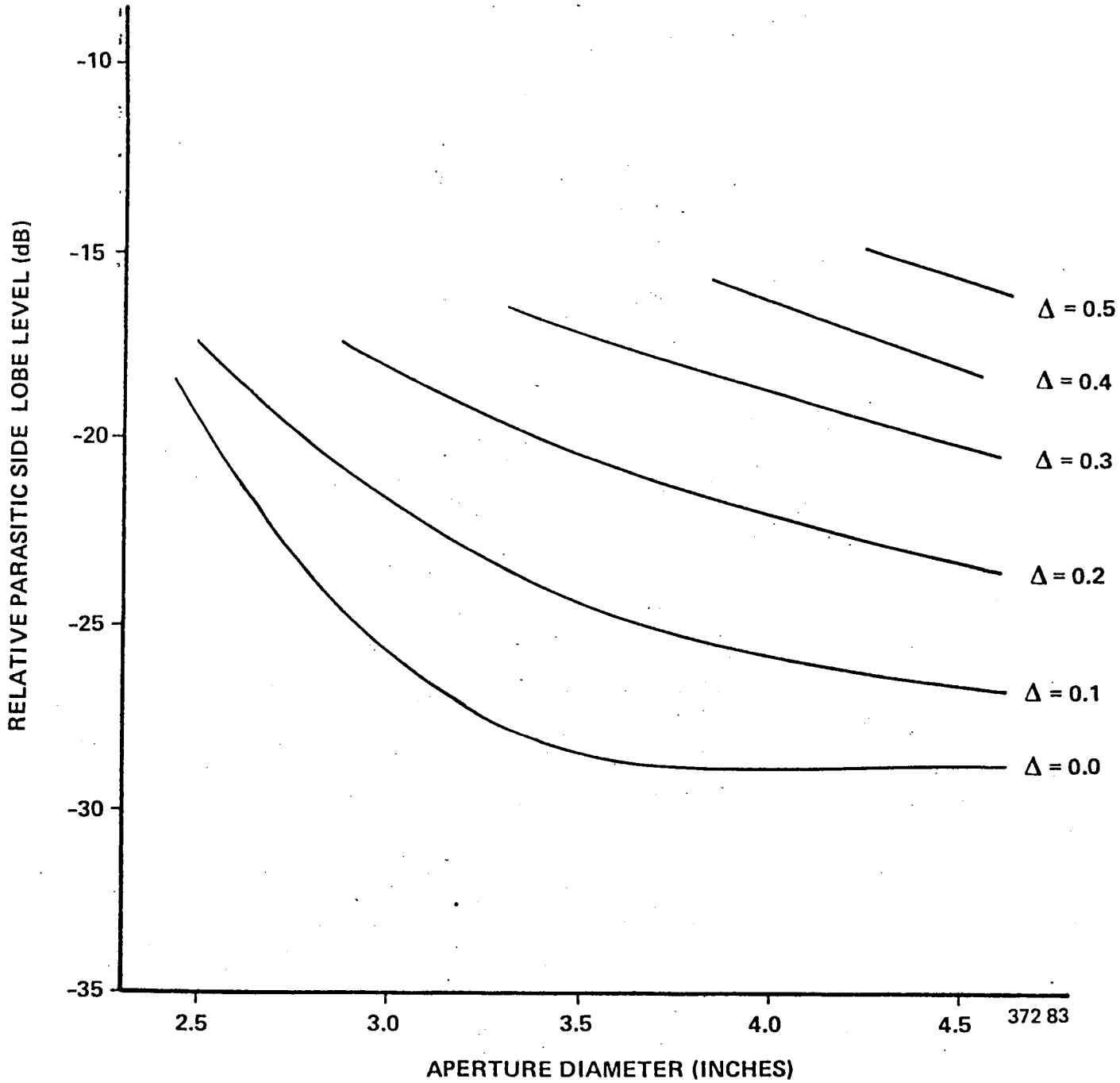

Figure 57. Relative PSLL Versus Aperture Diameter

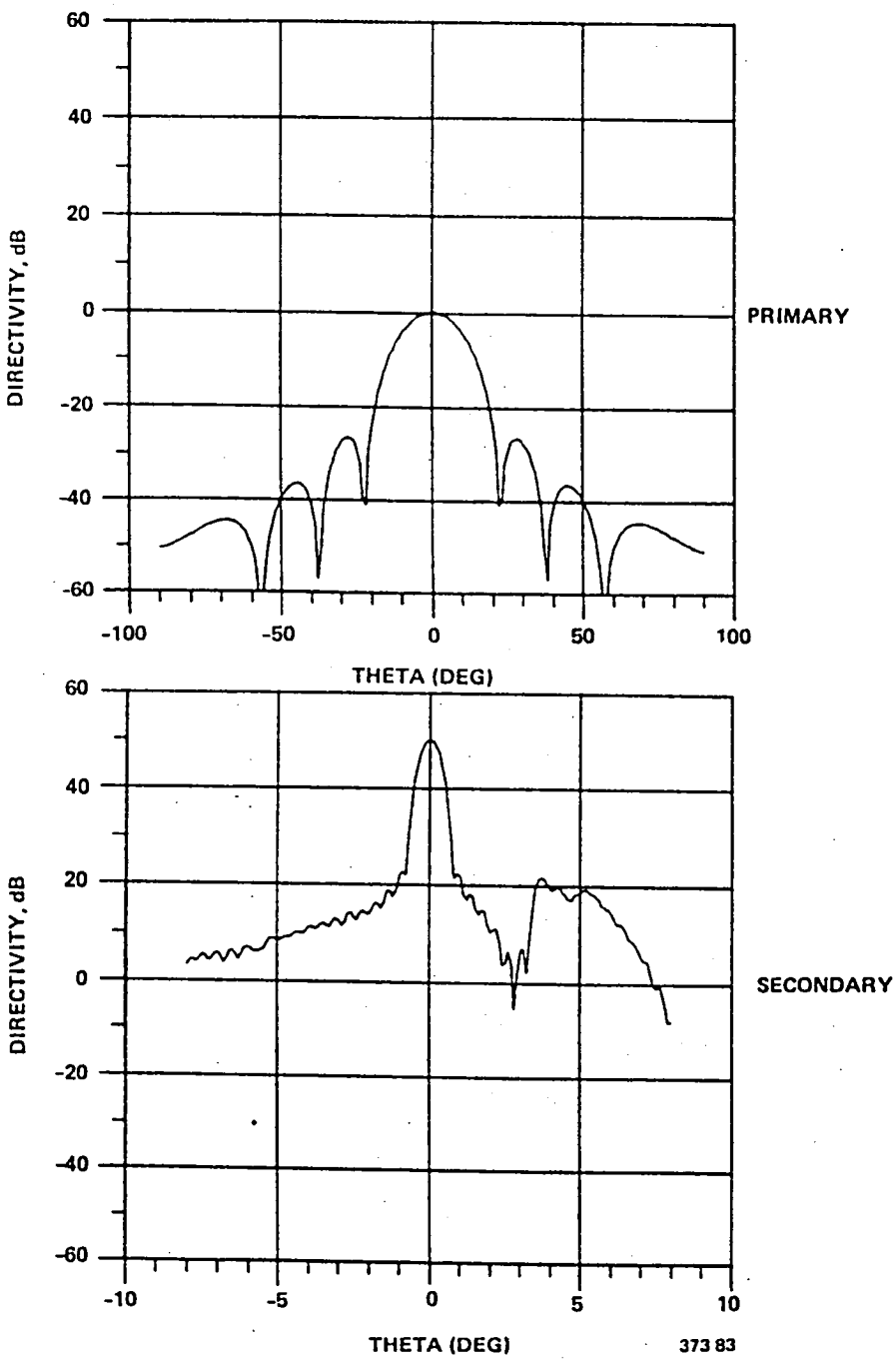

Figure 58. Corrugated Horn, $\Delta = 0.0$ D = 3.5"

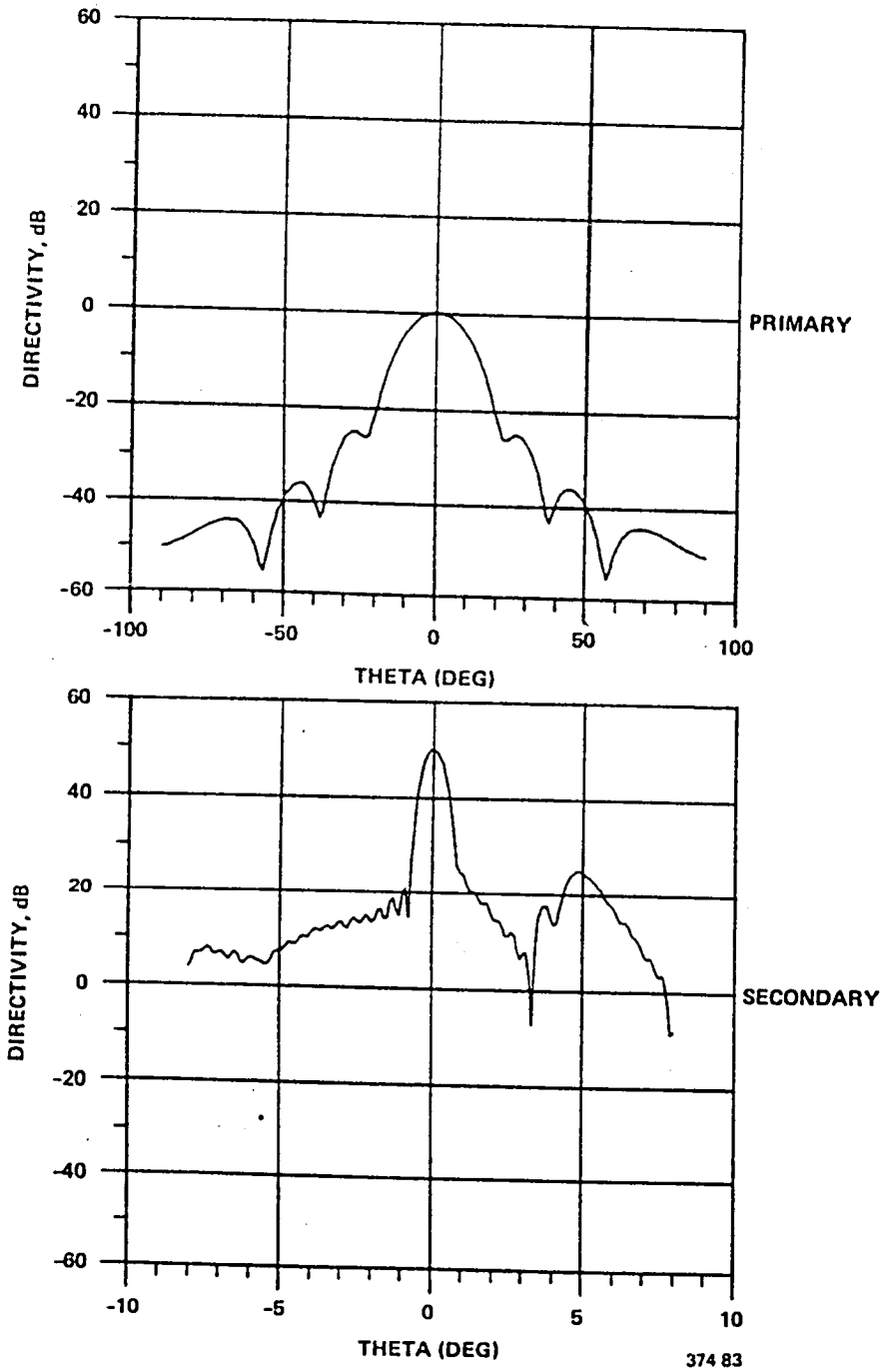

Figure 59. Corrugated Horn, $\Delta = 0.1$ D = 3.5"

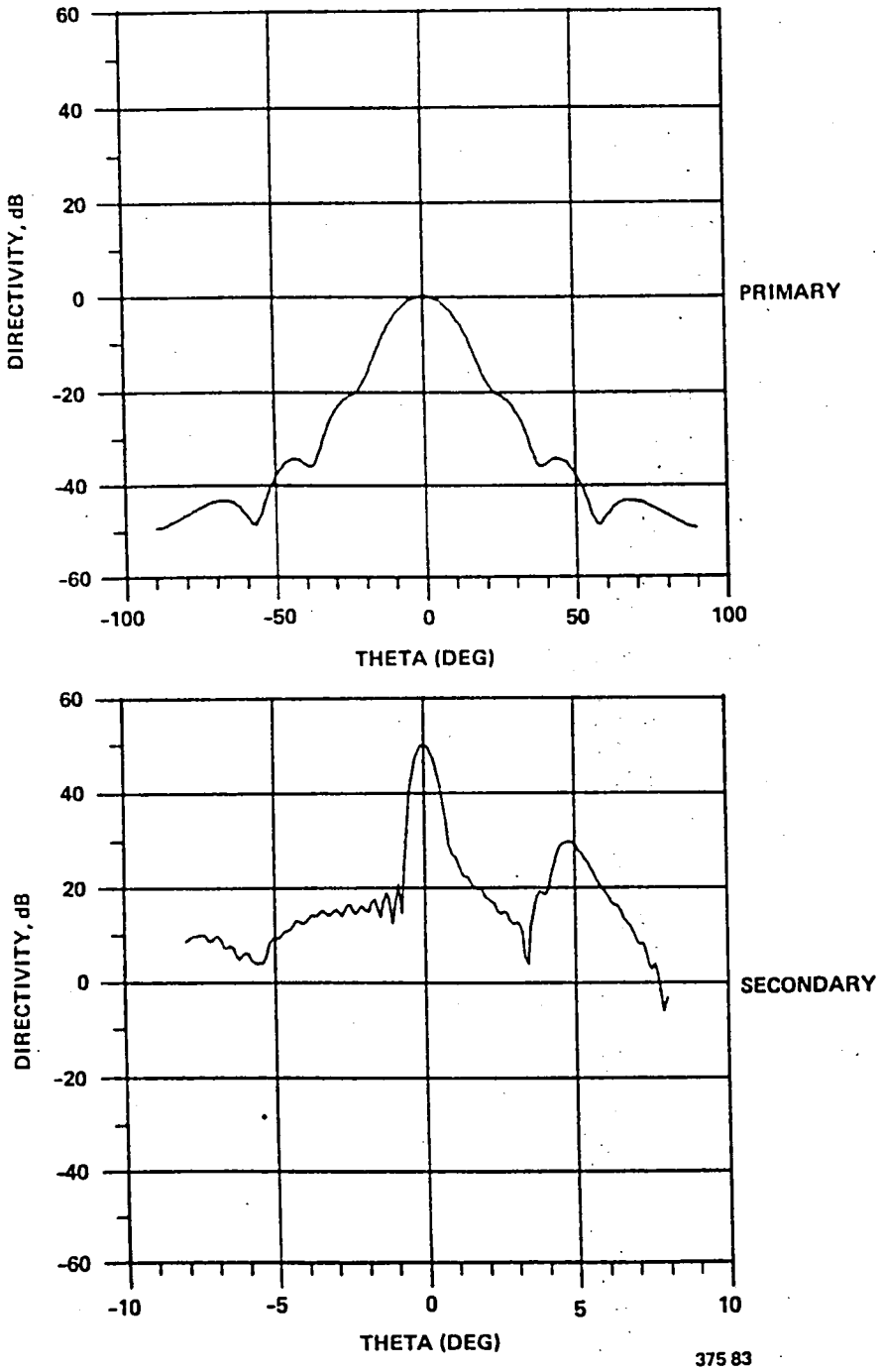

Figure 60. Corrugated Horn, $\Delta = 0.2$ D = 3.5"

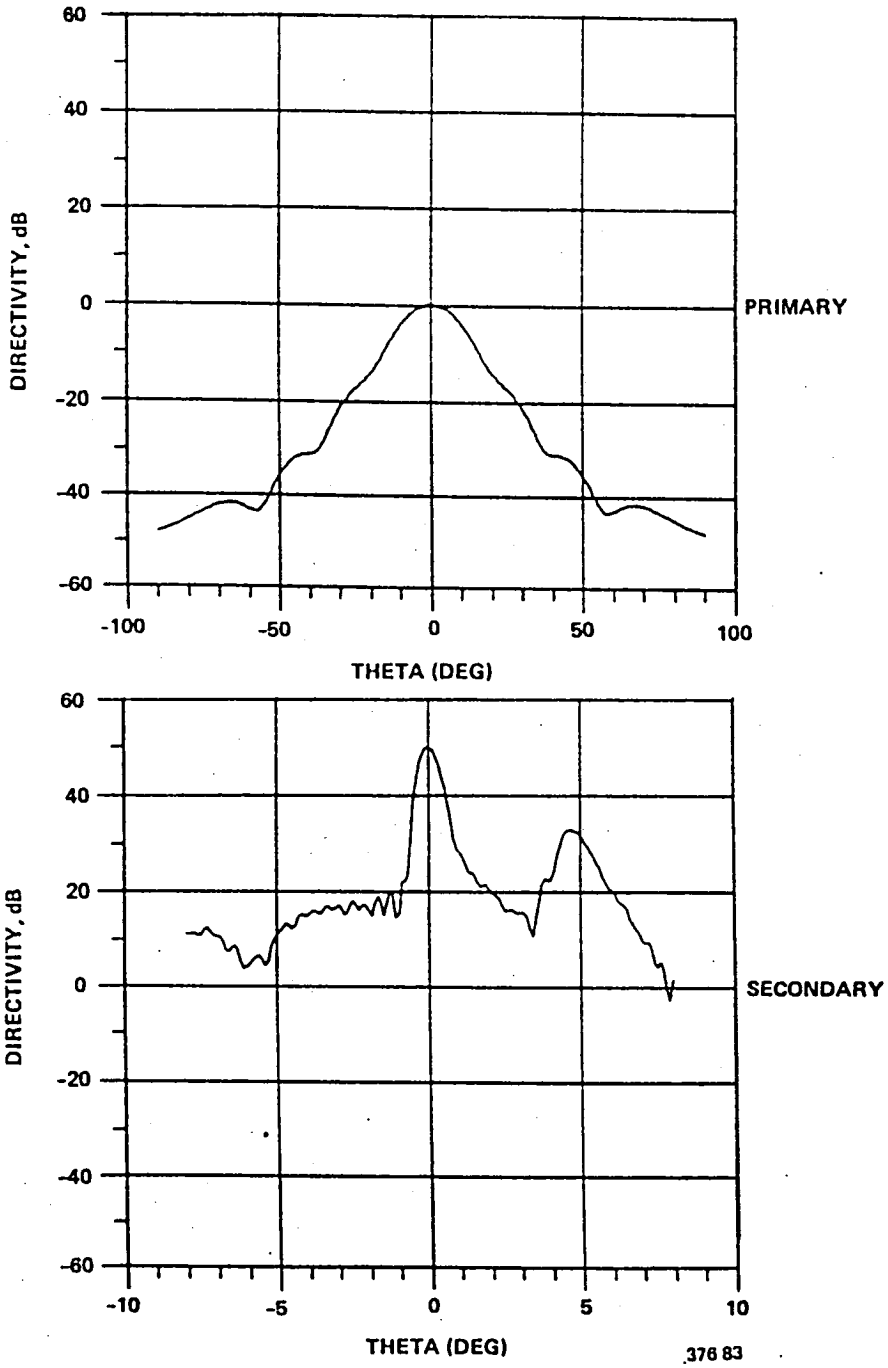

Figure 61. Corrugated Horn, $\Delta = 0.3$ D = 3.5"

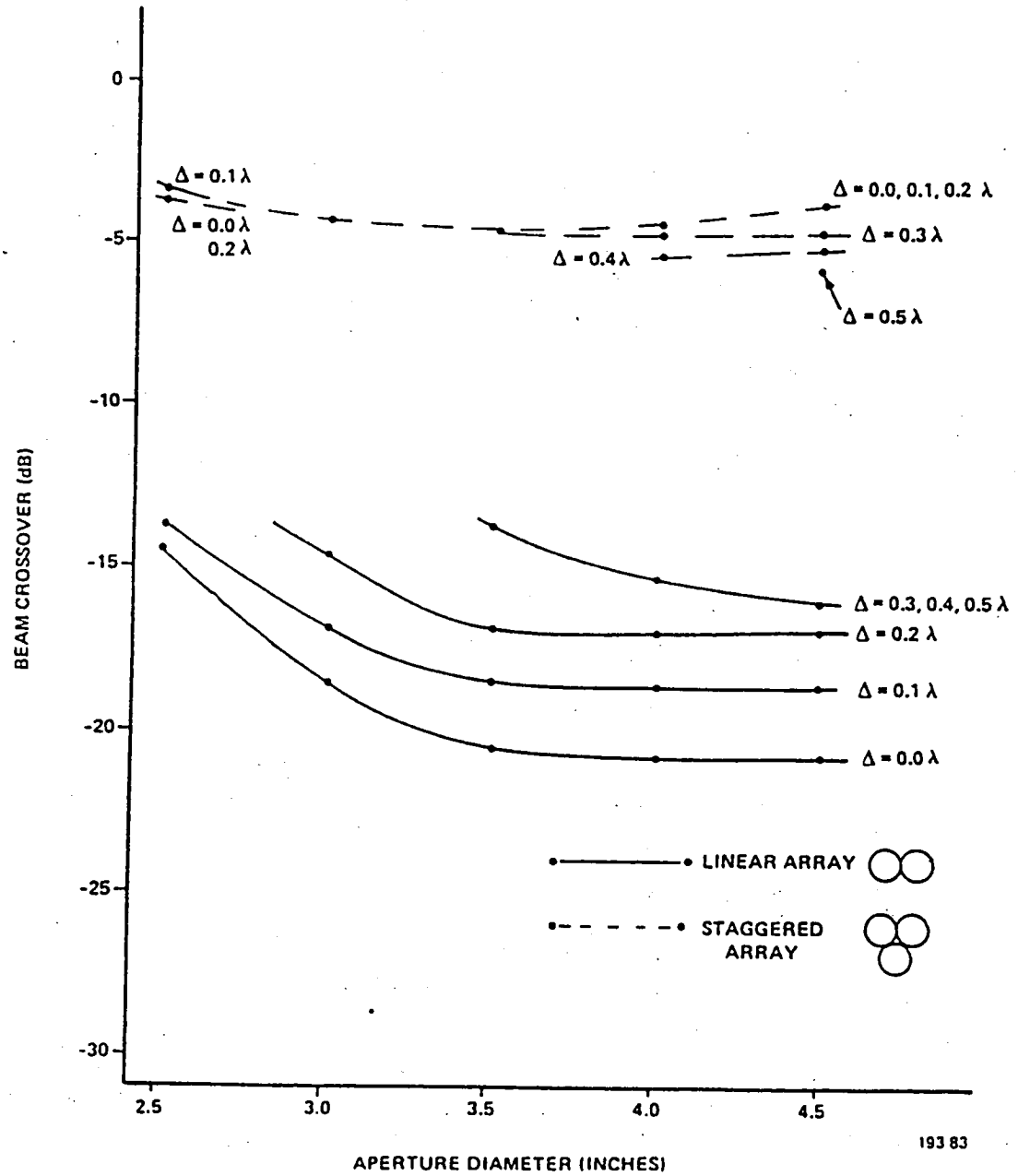

Figure 62. Corrugated Horn - Beam Crossover Level Versus Aperture Diameter

Another performance criterion of concern is the level at which the beams of adjacent feed elements cross in the far field. Assuming that the feed horns are placed as close to each other as possible, the beam crossover level was determined for the corrugated horn designs under consideration. In Figure 62, the results of this investigation are shown for both a linear array of horns and a staggered array. The crossover level appears to be unacceptable in all cases for the linear array, while acceptable in most cases for the staggered array. A linear type array is required for communications/spot beam applications where coverage is required at all points of interest simultaneously. The staggered array could be used in a radiometric application where "time-averaged" coverage is satisfactory.

USE OF DUAL MODE HORNS AS FEED ELEMENTS

Another common horn type which can be designed to have very symmetric E- and H-plane patterns, is the dual-mode horn. In this type of horn, TE_{11} and TM_{11} modes are mixed to produce a symmetrical pattern. The amount of TM_{11} mode present is varied so that the E-plane pattern (which is affected by TM_{11}) is matched to the H-plane (which TM_{11} does not affect). This technique can be implemented in conical or pyramidal horns (although some other modes are present in the pyramidal designs). The horns analyzed in this study were conical.

The initial dual mode design was chosen so that the first null of the H-plane pattern fell in the edge region of the reflector. The mode mix was then varied until the E-plane closely matched the H-plane over the reflector. The diameter of this horn was 4.5λ, or about 3.54 inches. The primary antenna pattern for this design is shown in Figure 63. The far-field pattern of the quadrant reflector system was computed using the 4.5λ dual mode horn

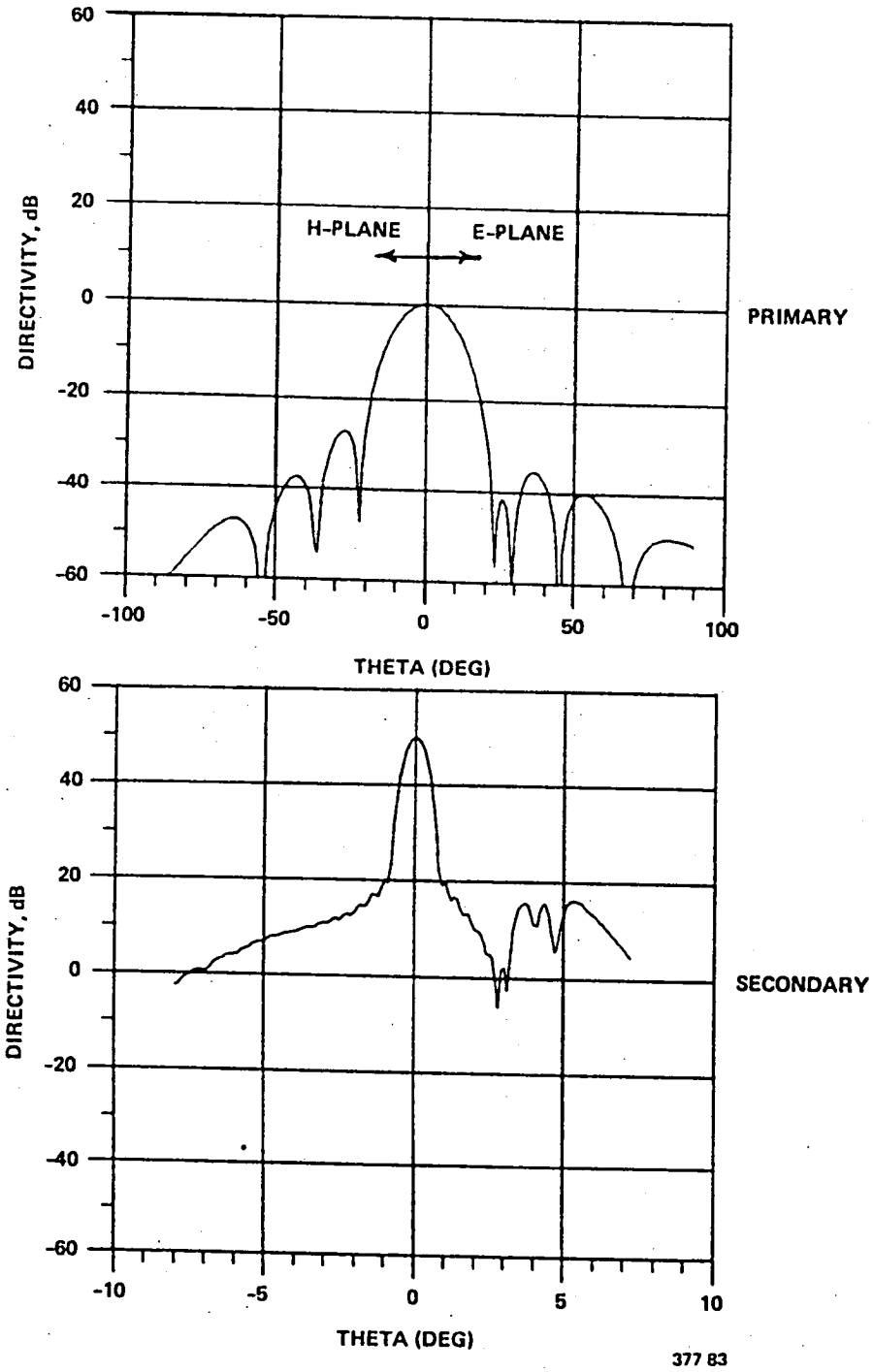

Figure 63. 4.5 λ Dual Mode Horn

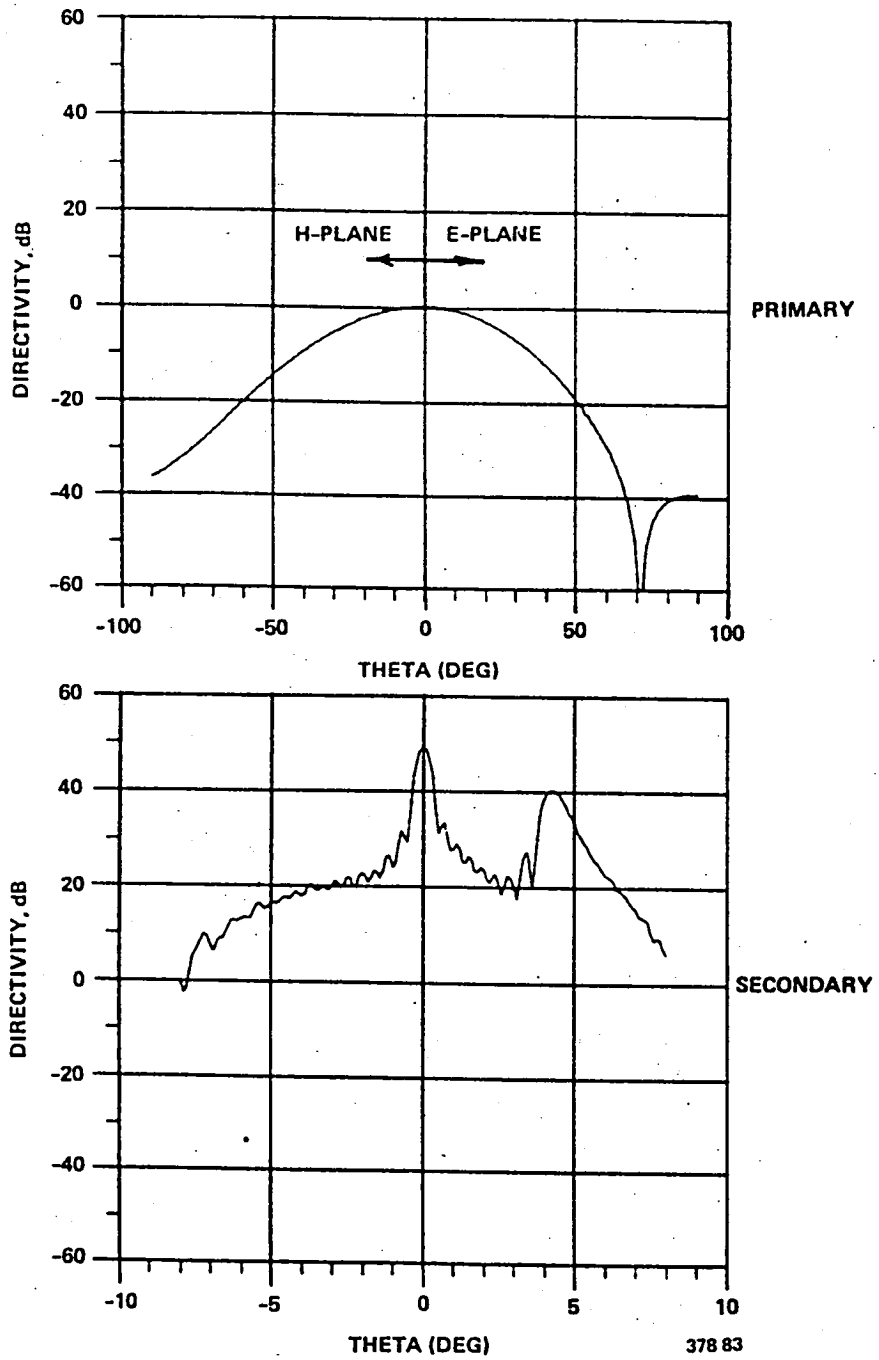

Figure 64. 1.5 λ Dual Mode Horn

as the feed. Figure 63 also shows the results of this analysis, which include the quite low parasitic side lobe level of around -33 dB.

A second dual mode design was taken under consideration. This horn was 1.5λ, or 1.18 inches, in diameter. It was selected not for its performance as a single horn feed, but for its potential use in a cluster feed design. A seven horn cluster composed of these horns would fit in approximately the same space as the 4.5λ horn. The principal planes of the primary pattern are shown in Figure 64. As a matter of interest, a secondary singlet pattern was computed using this horn as a reflector feed. The parasitic side lobe level for this horn, with its broad primary pattern, was very high, as expected. These results are also given in Figure 64.

Based on these results, and the fact that a typical seven horn cluster of such horns will have grating lobes striking the parasitic reflectors, it has not been established that clusters of 1.5λ elements are suitable for the quad aperture designs.

USE OF FEEDS WITH SYNTHESIZED APERTURE DISTRIBUTIONS

Apparently, the desired primary pattern for the quadrant reflector system is a circularly symmetric, low side lobe pattern with its first null at around 21°. There exist several window functions whose Fourier transforms meet the symmetry and side lobe requirements. By synthesizing these windows as an aperture distribution, and adjusting the size of the aperture in order to place the first null at the edge of the primary illuminated reflector, a feed pattern which will yield very good far-field secondary patterns is possible to attain. The problem of synthesizing these aperture distributions is not addressed here, but it could be accomplished by some version of a cluster feed.

Table III. Aperture Distributions

SCIAMBI

$$A + B\left(1.0 - \left(\frac{n-1}{N-1}\right)^2\right)^P$$

BOHMAN

$$\left(1.0 - \left|\frac{n-1}{N-1}\right|\right)\cos\left(\pi\left|\frac{n-1}{N-1}\right|\right) + \frac{1}{\pi}\sin\left(\pi\left|\frac{n-1}{N-1}\right|\right)$$

BLACKMAN

$$0.42 + 0.50\cos\left(\pi\left(\frac{n-1}{N-1}\right)\right) + 0.08\cos\left(2\pi\left(\frac{n-1}{N-1}\right)\right)$$

EXACT BLACKMAN

$$0.42659071 + 0.49656062\cos\left(\pi\left(\frac{n-1}{N-1}\right)\right) + 0.07684867\cos\left(2\pi\left(\frac{n-1}{N-1}\right)\right)$$

HAMMING

$$0.54 + 0.46\cos\left(\pi\left(\frac{n-1}{N-1}\right)\right)$$

RIESZ

$$1.0 - \left(\frac{n-1}{N-1}\right)^2$$

N = TOTAL NUMBER SAMPLE POINTS

$0 \leq n \leq N$

Table IV. Synthesized Aperture Distributions - Test Results

Aperture Distribution	Diameter (Wavelengths)	Diameter (Inches)	Peak Gain Secondary (dB)	Parasitic Side Lobe Level Secondary (dB Relative to Peak)
Sciambi - A = 0.0, P = 2.5	5.08	4	50.50	-28.46
A = 0.1, P = 2.5	5.08	4	49.87	-33.58
A = 0.1, P = 2.5	6.35	5	48.32	-40.35
A = 0.1, P = 2.5	7.62	6	46.80	-39.83
A = 0.1, P = 2.5	8.89	7	45.43	-37.92
A = 0.1, P = 2.5	10.16	8	44.24	-37.46
A = 0.1, P = 2.5	11.43	9	43.23	-38.06
A = 0.1, P = 2.5	12.70	10	42.26	-38.05
A = 0.1, P = 2.5	5.08	4	49.12	-32.16
A = 0.2, P = 2.5	5.08	4	48.34	-30.25
Bohman	7.62	6	49.04	-40.58
	8.89	7	47.86	-48.67
Blackman	7.62	6	48.83	-42.03
	8.89	7	47.63	-51.65
	10.16	8	46.49	-58.92
Exact Blackman	8.89	7	47.52	-53.99
	10.16	8	46.39	-63.52
Hamming	6.35	5	48.37	-44.74
Riesz	5.08	4	48.61	-26.70

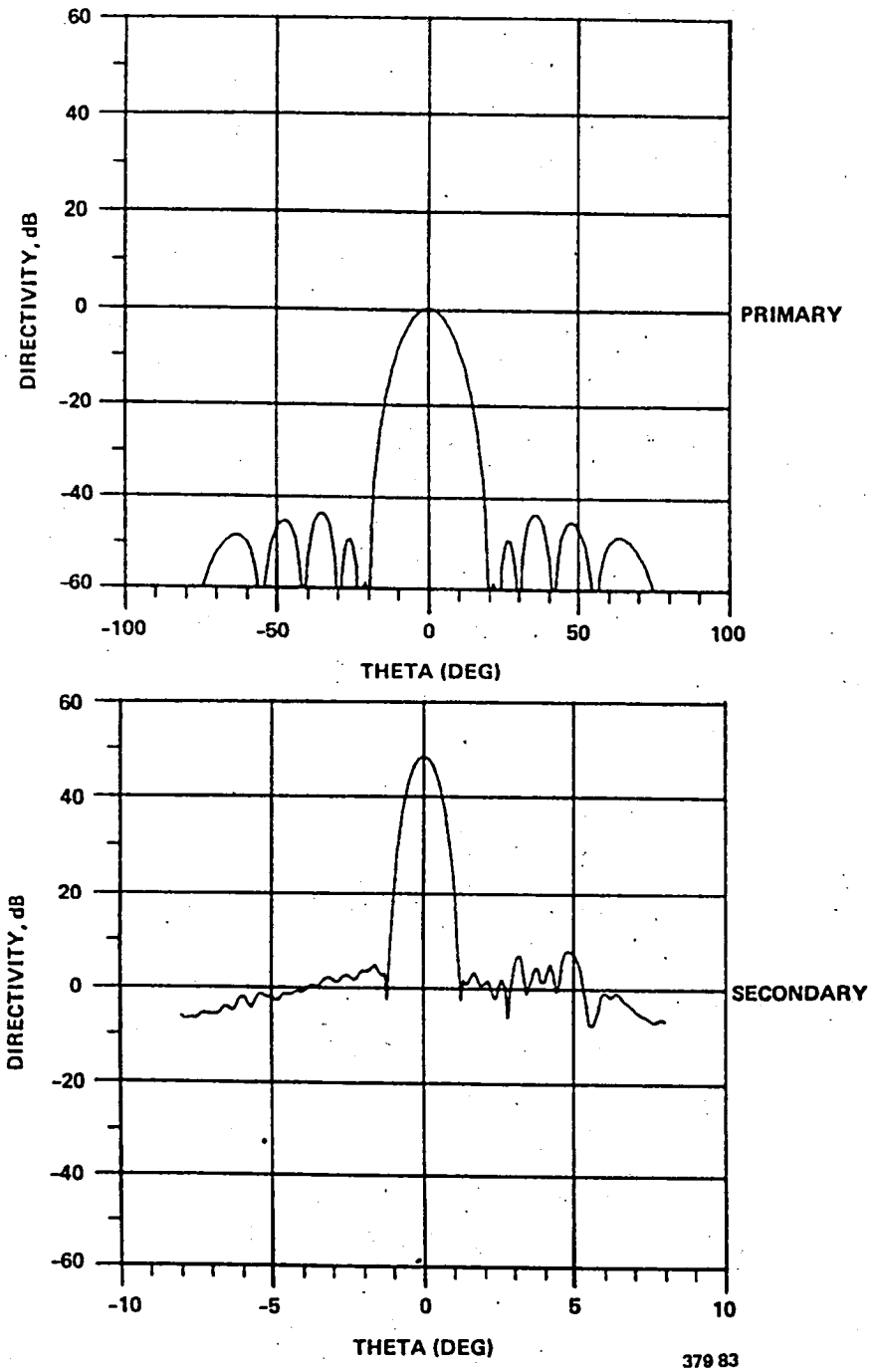

Figure 65. Sciambi Distribution, A = 0.1, P = 2.5, D = 5"

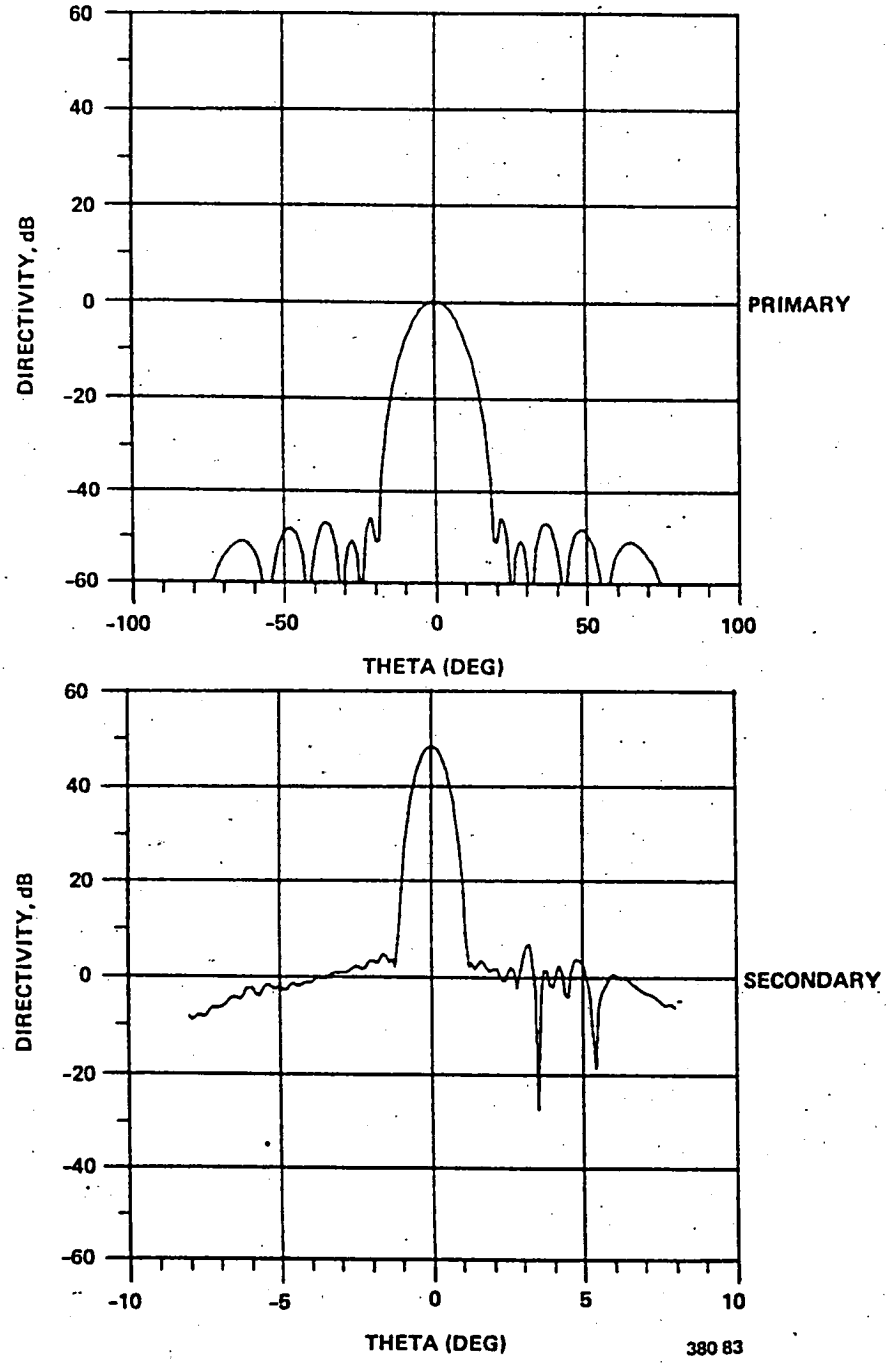

Figure 66. Hamming Distribution D = 5"

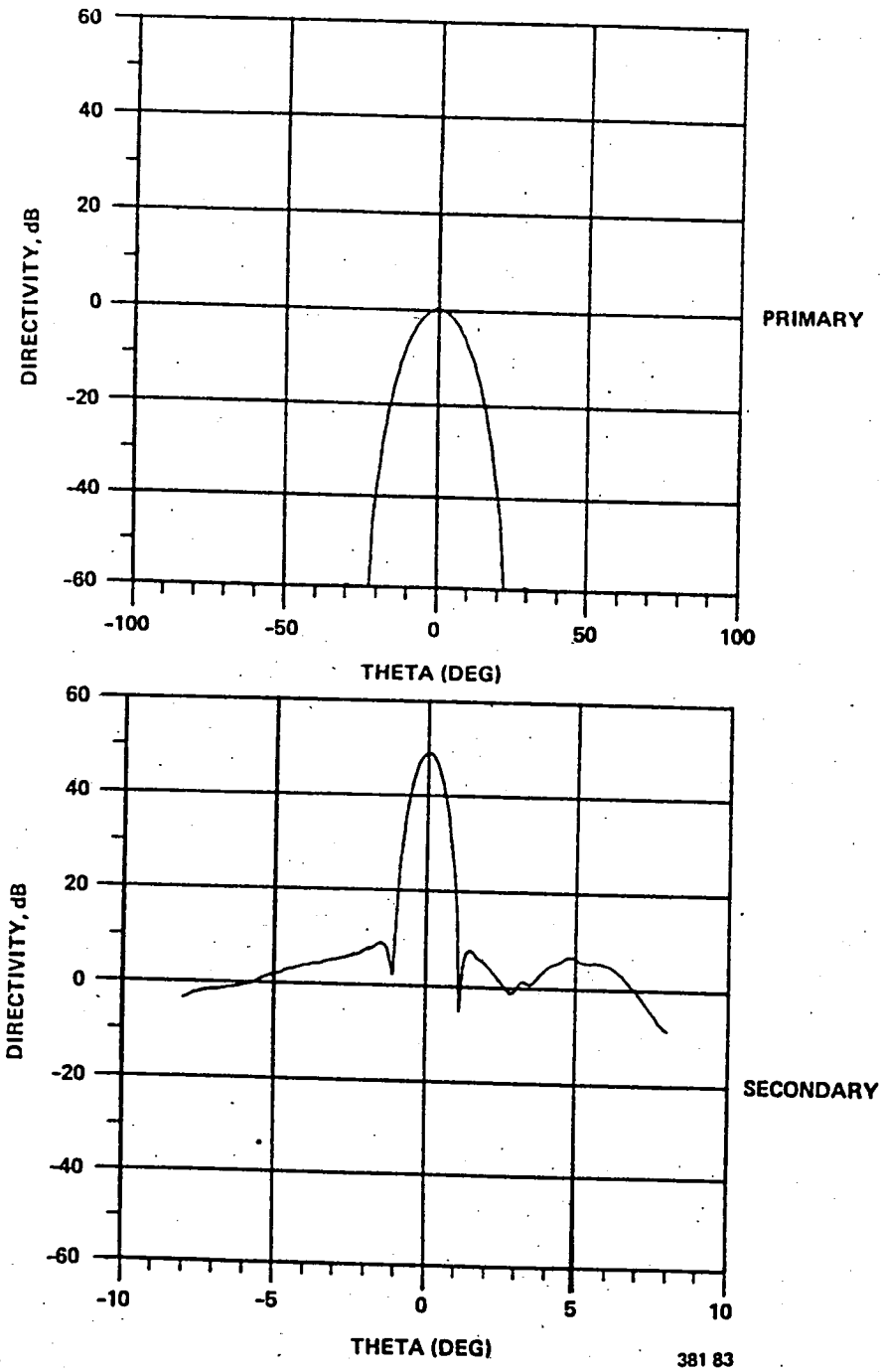

Figure 67. Blackman Distribution D = 6"

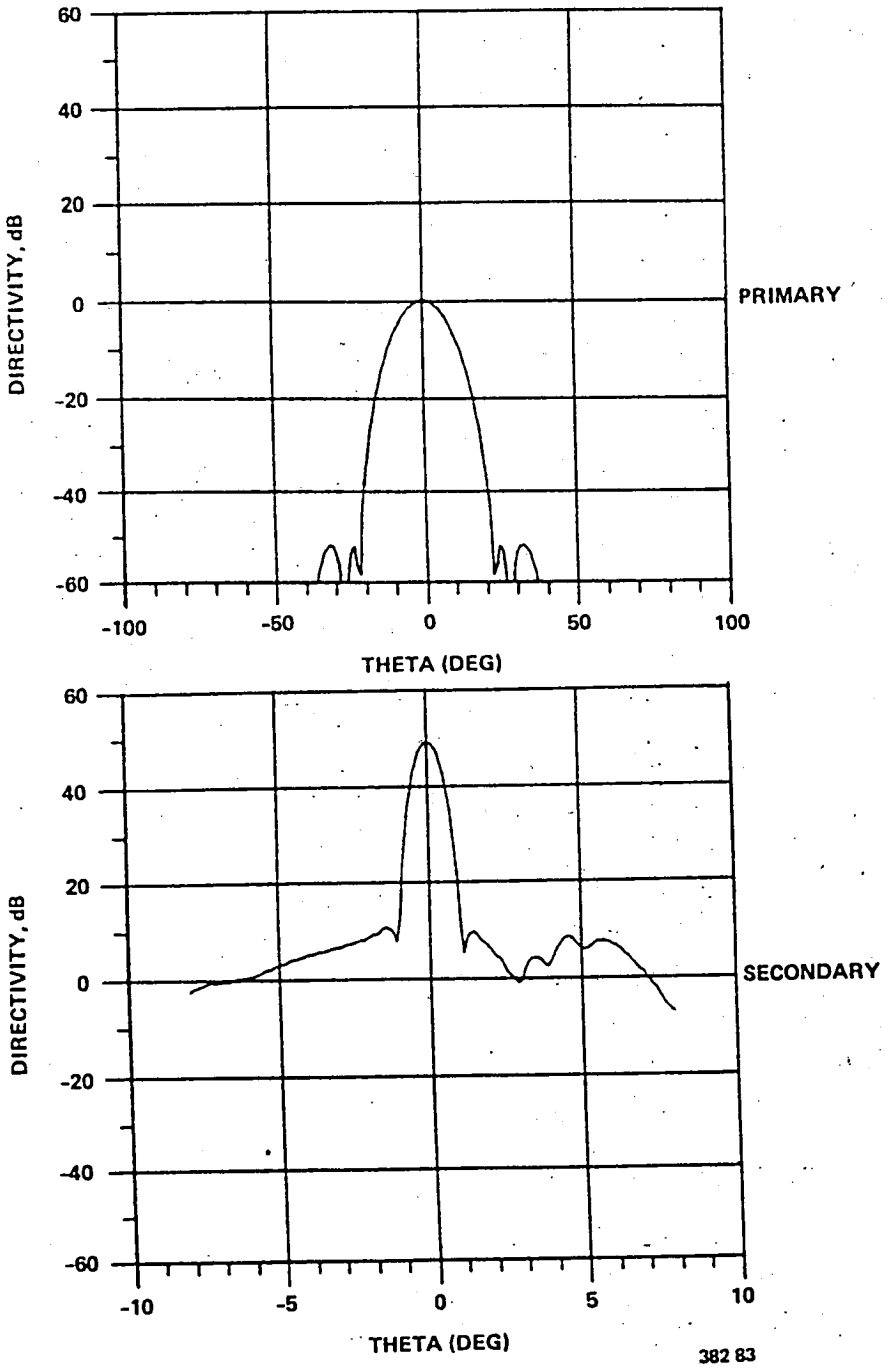

Figure 68. Bohman Distribution D = 6"

A list of the window functions used in this phase of the investigation, along with their governing equations, is given in Table III.

The first distribution considered was the Sciambi window. It is a very good approximation to the Taylor distribution (especially when $A = 0.1$). An aperture diameter of 4 inches was chosen for initial study since it gave a null near 21° for all values of A and P under consideration. As the best performance, in terms of gain and parasitic side lobe level, was achieved by a distribution with $P = 2.5$, $A = 0.1$, these values were chosen for more extensive study. The results of this analysis are given in Table IV. These findings established that the same criteria for good secondary far-field performance held for synthesized aperture distributions as well as for standard horn types.

Having determined this, only those aperture diameters giving a null in the vicinity of 21° were considered when investigating the other windows. The results of these further studies are also given in Table IV. Some representative primary and secondary patterns are shown in Figures 65 through 68.

Note that there are several designs which yield good results. However, these are gained using ideal distributions with no aperture phase error. Therefore, the use of window functions deserves further and more practical study.

DISCUSSION OF FEED DESIGNS FOR QUAD APERTURE RELECTORS

The computed results presented in the aperture synthesis section clearly indicate that equivalent feed apertures of at least 4.5λ to 6λ in diameter are required to obtain low side lobe performance from the quad aperture configuration considered. There are several equivalent aperture distributions of varying types which, if synthesized well, can produce a secondary pattern performance of good quality for both radiometric and communications applications.

From other work, Harris has found that in order to achieve a performance similar to that required here, control of the cluster feed network must be on the order of ±0.1 dB and ±2° to maintain the cluster pattern performance desired. Analyses and computer programs are available at Harris to synthesize these aperture distributions including weight amplitude and phase determination. Such analyses are also very valuable in predicting the effects of hardware construction errors and deviation from ideal performance by feed networks and devices.

The well established cluster feed analysis method and design techniques have to be modified for this application. Cluster elements must be used where cluster element spacings will not result in grating lobes that impinge upon the parasitic reflectors in the design arrangement.

CONCLUSIONS

The most significant result of this study was the demonstration of the existance of the parasitic lobe in the quad aperture design, and the quantification of the amplitude and location of these lobes through analyses and measurements.

The measurements of the scaled dielectric cords revealed that little energy is scatterd in the forward region of the antenna pattern. Little difference in far-field reflector patterns were noted by overlaying measured patterns, with and without dielectric cords, over a ±6° by ±45° sector. For many communications applications, lobes outside of this sector, as seen from stationary earth orbit, are relatively unimportant.

The agreement between analysis and measurement for the single quad aperture is quite good. The differences between theory and measurement for the double quad aperture are believed to be due to inadequate modeling of the feed horns outside of the 25° conic sector where the horns were designed to

have rotationally symmetric far-field patterns. Where synthesized symmetric feed patterns, such as those produced by cluster feeds are used, it is shown that excellent parasitic and other wide angle side lobe performance can be achieved with the quad aperture hoop column design.

Cluster designs can be developed which match the desired synthesized aperture distributions. Indeed, proven analytical methods are available at Harris to rapidly converge on proper feed weighted networks. The use of this design capability and the quad aperture codes allow the accurate study of different system applications such as radiometry and communications. Other useful extensions of these verified analytical techniques include shape distortion, pillow effects, and inclusion of scattering from the central mast.

REFERENCES

1. Y. Rahmat-Samii and V. Galindo-Isreal, "Shaped Reflector Antenna Analysis using the Jacobi-Bessel Series," IEEE Trans. on Antennas and Propagation, Vol. AP-28, No. 4, July 1980.

2. A. Ludwig, "The Definition of Cross Polarization," IEEE Trans. on Antennas and Propagation, Vol. AP-21, No. 1, January 1973.

1. Report No.	2. Government Accession No.	3. Recipient's Catalog No.
NASA CR-172413		

4. Title and Subtitle	5. Report Date
Hoop Column Antenna - RF Verification Model Volume II - Analysis and Correlation	August 1984
	6. Performing Organization Code
7. Author(s)	8. Performing Organization Report No.
W. F. Croswell (Editor), M. D. Vanstrum, R. J. Schrimpf, R. G. Taylor, and R. L. Moye	
	10. Work Unit No.
9. Performing Organization Name and Address	11. Contract or Grant No.
Harris Corporation Government Electronic Systems Division P. O. Box 9400 Melbourne, FL 32902	NAS 1-15763
	13. Type of Report and Period Covered
12. Sponsoring Agency Name and Address	Contractor Report Jan. to Aug. 1983
National Aeronautics and Space Administration Washington, DC 20546	14. Sponsoring Agency Code
	506-62-43-01

15. Supplementary Notes

Langley Research Center Technical Monitor: Thomas G. Campbell
Final Report

16. Abstract

As part of the Large Space System Technology Program, this report, in two volumes, presents the theoretical and experimental results of the RF characteristic of a hoop/column, quad aperture antenna using an RF verification model.

To satisfy the primary purposes of the model it provides experimental pattern data for the quad aperture configuration at different reflector edge illumination levels, from which the geometry and edge effects can be assessed, and provides experimental data which can be compared with calculations using various theoretical reflector scattering formulae. It also experimentally determines the effects upon secondary patterns of scale model quartz cables, as used in the hoop/column design, upon secondary patterns in order to assess the importance of developing a scattering theory to predict such effects. In addition, this report contains a comprehensive theoretical study and the experimental pattern results of quad aperture antenna feeds, a discussion of the fundamental affect of parasitic side lobes, their amplitude, and location in space.

17. Key Words (Suggested by Author(s))	18. Distribution Statement
Antenna Parabolic Reflector Quad Aperture Hoop/Column Feeds	Unclassified - Unlimited Subject Category 32

19. Security Classif. (of this report)	20. Security Classif. (of this page)	21. No. of Pages	22. Price
Unclassified	Unclassified	77	A05

For sale by the National Technical Information Service, Springfield, Virginia 22161 NASA-Langley, 1984

151A

R10

DO NOT REMOVE SLIP FROM MATERIAL

Delete your name from this slip when returning material to the library.

NAME	MS
~~Italiano~~	~~HLG~~
Library	185

NASA Langley (Rev. May 1988) RIAD N-75